Miner Deposita (2009) 44:415–434
DOI 10.1007/s00126-008-0221-3

ARTICLE

A geochemical study of the Sweet Home Mine, Colorado Mineral Belt, USA: hydrothermal fluid evolution above a hypothesized granite cupola

Volker Lüders · Rolf L. Romer · H. Albert Gilg · Robert J. Bodnar · Thomas Pettke · Dean Misantoni

Received: 23 July 2008 / Accepted: 20 October 2008 / Published online: 26 November 2008

Abstract Deposition of quartz–molybdenite–pyrite–topaz–muscovite–fluorite and subsequent hübnerite and sulfide–fluorite–rhodochrosite mineralization at the Sweet Home Mine occurred coeval with the final stage of magmatic activity and ore formation at the nearby world-class Climax molybdenum deposit about 26 to 25 m.y. ago. The mineralization occurred at depths of about 3,000 m and is related to at least two major fluid systems: (1) one dominated by magmatic fluids, and (2) another dominated by meteoric water. The sulfur isotopic composition of pyrite, strontium isotopes and REY distribution in fluorite suggest that the early-stage quartz–molybdenite–pyrite–topaz–muscovite–fluorite mineral assemblage was deposited from magmatic fluids under a fluctuating pressure regime at temperatures of about 400°C as indicated by CO_2-bearing, moderately saline (7.5–12.5 wt.% NaCl equiv.) fluid inclusions. LA-ICPMS analyses of fluid inclusions in quartz demonstrate that fluids from the Sweet Home Mine are enriched in incompatible elements but have considerably lower metal contents than those reported from porphyry–Cu–Au–Mo or Climax-type deposits. The ore-forming fluid exsolved from a highly differentiated magma possibly related to the deep-seated Alma Batholith or distal porphyry stock(s). Sulfide mineralization, marking the periphery of Climax-type porphyry systems, with fluorite and rhodochrosite as gangue minerals was deposited under a hydrostatic pressure regime from low-salinity±CO_2-bearing fluids with low metal content at temperatures below 400°C. The sulfide mineralization is characterized by mostly negative $\delta^{34}S$ values for sphalerite, galena, chalcopyrite, and tetrahedrite, highly variable $\delta^{18}O$ values for rhodochrosite, and low REE contents in fluorite. The Pb isotopic composition of galena as well as the highly variable $^{87}Sr/^{86}Sr$ ratios of fluorite, rhodochrosite, and apatite indicates that at least part of the Pb and Sr originated from a much more radiogenic source than Climax-type granites. It is suggested that the sulfide mineralization at the Sweet Home Mine formed from magmatic fluids that mixed with variable amounts of externally derived fluids. The migration of the latter fluids, that were major components during late-stage mineralization at the Sweet Home Mine, was probably driven by a buried magmatic intrusion.

Keywords Mo porphyry deposits · Climax · Sweet Home · Colorado Mineral Belt · Rhodochrosite · Fluid inclusions · Stable isotopes · Lead isotopes · Strontium isotopes

Editorial handling: B. Lehmann

V. Lüders (✉) · R. L. Romer
GeoForschungsZentrum Potsdam,
Telegrafenberg,
14473 Potsdam, Germany
e-mail: volue@gfz-potsdam.de

H. A. Gilg
Lehrstuhl für Ingenieurgeologie, TU München,
Arcisstr. 21,
80290 Munich, Germany

R. J. Bodnar
Department of Geosciences, Virginia Tech,
Blacksburg, VA 24061, USA

T. Pettke
Institute of Geological Sciences, University of Bern,
Baltzerstrasse 1 + 3,
CH-3012 Bern, Switzerland

D. Misantoni
Colorado Calumet Company Inc.,
P.O. Box 1169, Golden, CO 80402, USA

Introduction

The Colorado Mineral Belt (COMB) hosts some of the largest and economically most important molybdenum deposits in the world. The emplacement of Climax-type granites (White et al. 1981) and the formation of porphyry molybdenum deposits is related to incipient extension related to the development of the Rio Grande rift system (e.g., Wallace et al. 1968; Wallace 1995). Porphyry molybdenum deposits are thought to have formed from leucogranitic magmatic fluids that were high in fluorine and produced large-scale silicification and precipitation of quartz veins above the magmatic stocks (e.g., White et al. 1981; Bookstrom et al. 1988). In general, Climax-type deposits are characterized by stockwork molybdenite+quartz±K-feldspar±biotite±fluorite±topaz± pyrite±magnetite veinlets and fracture fillings that occur throughout hydrothermally altered and intensively fractured stockworks of highly evolved leucogranitic porphyries (Wallace et al. 1968; 1978; Westra and Keith 1981; White et al. 1981; Stein and Hannah 1985; Wallace 1995; Seedorff and Einaudi 2004a, b). Locally, mineralization in the form of hübnerite ($MnWO_4$, abundant at Climax) and base metal mineralization mostly occur above the cupolas of intrusives or on the flanks (e.g., Wallace et al. 1968; Bookstrom et al. 1988; White et al. 1981; Seedorff and Einaudi 2004a, b). Previous studies have suggested that Climax-type porphyry systems, including their peripheral hydrothermal base metal deposits, are of magmatic origin and periods of ore deposition have been attributed to specific magmatic events (Seedorff and Einaudi 2004b; Klemm 2006). For the giant molybdenum porphyry deposits of Climax and Urad-Henderson, both located in the COMB, evidence for significant wall-rock alteration or redistribution of metals within the deposits by meteoric waters is not observed (Stein and Hannah 1985; Stein 1988; Seedorff and Einaudi 2004b). At Climax, wall-rock alteration has been attributed to magmatic fluids (Stein 1988) although Hall et al. (1974) favored a mixing model of isotopically light (meteoric) and heavy (magmatic) waters for the formation of the hydrothermal orebodies. In addition to the Climax-type deposits, the COMB also hosts a variety of Au–Ag–Pb–Cu–Zn lode deposits as well as other molybdenum-bearing mineralizations (for locations and details see Wallace 1995) of minor economic importance (Fig. 1). Among these deposits, the Sweet Home Mine is characterized by a mineral paragenesis that includes base metal sulfides and sulfosalt (tetrahedrite–tennantite) assemblages typically occurring in vein structures in the Alma district (Fig. 1) as well as minor quartz–molybdenite mineralization, and hübnerite ore pockets. Historically, the Sweet Home Mine was a minor silver producer.

The Sweet Home Mine is best known for the superb rhodochrosite mineral specimens (Moore et al. 1998) that have been collected throughout all periods of mining activity and are exhibited in museums worldwide. The mine was operated from 1991 through 2004 specifically for mineral specimens and abundant sample material was provided by Collector's Edge, Golden, CO, for this study. This paper describes a detailed fluid inclusion study of minerals representing all mineralization stages at the Sweet Home Mine, using microthermometry, Raman spectroscopy, and laser-ablation ICPMS (LA-ICPMS) to characterize the chemical composition of the hydrothermal fluids and temperatures of mineral formation. We utilize U–Pb and Rb–Sr isotope systematics of host phases to estimate the duration of the local mineralizing processes. Furthermore, REE and yttrium distributions in fluorite and stable isotope geochemistry of rhodochrosite (O, C) and sulfides (S) are used to discriminate between possible fluid sources.

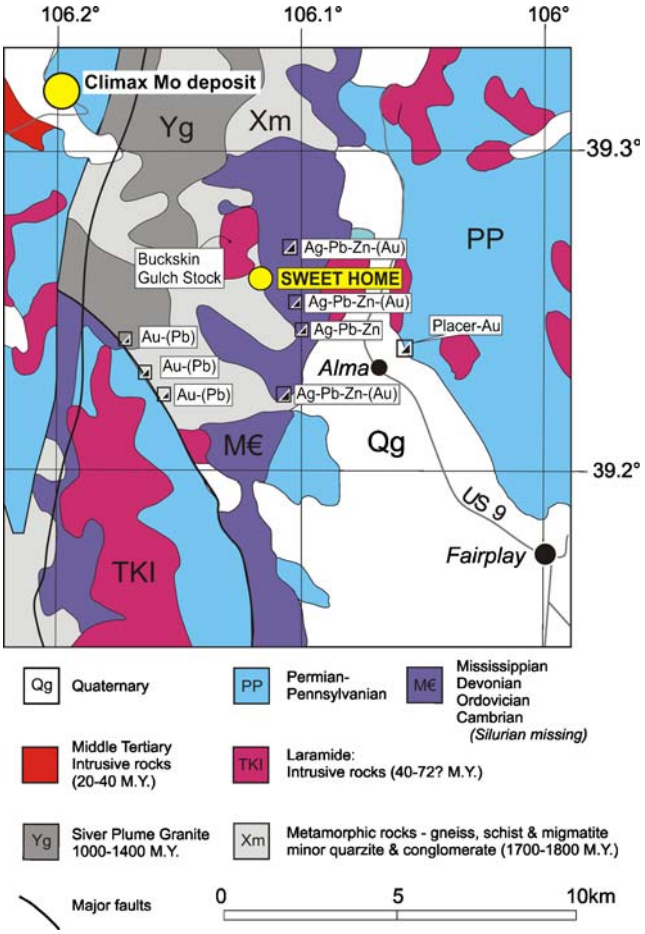

Fig. 1 Geological map showing the location of the Sweet Home Mine, the Climax Mo deposit, and other historical mining locations in the Mosquito Range of the Colorado Mineral Belt

Geology of the Sweet Home Mine

A detailed description on the geological setting of the Sweet Home Mine is given by Misantoni et al. (1998) and

Bartos et al. (2007), and is summarized here. The formation of Mo-bearing veins in the Alma district is assumed to have occurred concurrently with the final stage of ore deposition at Climax and is related to a last pulse of hydrothermal fluids from the inner dome of the underlying Alma Batholith at about 26 Ma (Bookstrom et al. 1987, 1988). The Climax deposit is assumed to be hosted in shallow cupolas on the western margin of a large granitic batholith beneath the Alma mining district (Bookstrom et al. 1987; Bookstrom 1989) that is located about 7.5 km northwest of the Sweet Home Mine. Although the Sweet Home Mine is located near several gold–silver–lead–zinc deposits, its mineral assemblages are similar to those of Climax molybdenum deposits. Previous workers have interpreted mineralization at the Sweet Home Mine as a "single pulse variant of a Climax-type hydrothermal system" where minerals precipitated from fluids of magmatic origin that slowly cooled and were diluted by minor amounts of meteoric water towards the end of the mineralization (Bartos et al. 2007). Veins at the Sweet Home Mine are hosted by granite, gneiss, migmatite, and pegmatite of the ~1.8 Ga Idaho Springs Formation (e.g., Stein and Crock 1990) which is locally overlain by Pennsylvanian sedimentary rocks (Fig. 1). A locally foliated intrusive plug of Precambrian granodiorite intrudes the metamorphic rocks. Minor dikes of pre-ore Tertiary quartz monzonitic to monzonitic porphyries intrude the Precambrian rocks, as do molybdenite-bearing quartz-orthoclase pegmatites, dated at 26.0±0.7 Ma (2σ) by $^{40}Ar/^{39}Ar$ age determinations on sericite (Barbá et al. 2005). This age is concordant with fission track ages of hydrothermally altered zircon from the Wallace stock and its related porphyry molybdenum orebody at the Climax deposit (Bookstrom 1989). A wide range of Tertiary intrusive rocks is exposed outside of the mine area (Fig. 1).

Hydrothermal alteration is widespread at the Sweet Home Mine, and includes local potassic alteration of the gneisses, widespread quartz–sericite–pyrite halos around the veins, and a regional propylitic alteration composed of chlorite–hematite–pyrite, which is not directly related to the veins. Quartz–sericite–plagioclase alteration can grade into silicification or greisen-type alteration that includes abundant muscovite with quartz–pyrite–fluorite and is the most prevalent vein-related alteration type. $^{40}Ar/^{39}Ar$ ages from sericite of this early mineralization stage fall in the range of 26.1±0.1 and 25.5±0.1 Ma (2σ; Barbá et al. 2005). These ages are consistent with a $^{206}Pb/^{238}U$ age of 25.7±0.3 Ma (2σ; Romer and Lüders 2006) for three hübnerite samples from a single crystal, indicating that the formation of early quartz–molybdenite–pyrite–topaz–muscovite–fluorite mineralization and the deposition of hübnerite occurred in a short time interval.

Mineralized structures are generally narrow, averaging only 5–10 cm, and rarely attaining widths up to 25 cm. There are three structural orientations: (1) a northwest-striking, southwest dipping set, parallel to the schistosity in strike, but dipping more steeply, (2) a northeast-striking, steeply dipping set, which hosts all of the productive veins, and (3) a late, (minor) north–south striking set. Widening of the structures occurs at deflections in strike and dip, with right-lateral oblique slip resulting in southwest-raking "ore shoots" or, with incomplete filling, open pockets.

Two distinct mineralization stages are present in the mine (Fig. 2); an early assemblage containing quartz–molybdenite–pyrite–topaz–muscovite–fluorite, and a later assemblage containing galena–sphalerite–tetrahedrite–bornite and other sulfides/sulfosalts, and fluorite–rhodochrosite. Calcite, barite, and apatite were the last minerals to form. Tungsten mineralization, in the form of hübnerite, and early black sphalerite are common. It is not clear whether these minerals are associated with the early mineralization stage or are transitional between the two main stages. Secondary copper minerals locally replace tetrahedrite.

Analytical techniques

Fluid inclusions in transparent minerals were measured by conventional microthermometry using a FLUID INC-adapted U.S.G.S. gas-flow heating/freezing system mounted on an Olympus BX50 microscope. The stage was calibrated with synthetic inclusions supplied by Synflinc (Sterner and Bodnar 1984). Fluid inclusions in tetrahedrite were studied using the same heating–freezing stage mounted on an Olympus BHSM-IR infrared microscope (Lüders 1996).

Gas-bearing inclusions were analyzed using a Jobin-Yvon Raman spectrometer equipped with an Olympus optical microscope and 50× and 80× long-working-distance objec-

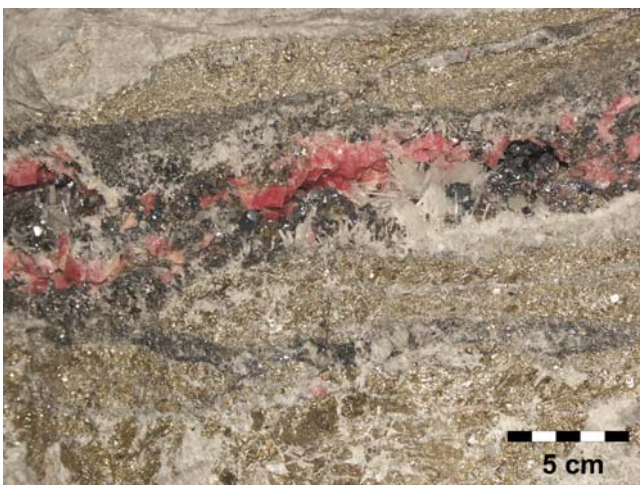

Fig. 2 Typical vein specimen from the Sweet Home Mine (Water Course Vein/Tedrahedrite drift # 24 in Fig. 3) showing massive pyrite and euhedral quartz crystals from the early stage and various sulfides and rhodochrosite from the main sulfide stage

tives. The exciting radiation used was a 532 nm Nd-YAG laser with a power of about 120 mW on the sample surface. Spectra were scanned twice in the wavelength range between 800 and 3,600 cm^{-1} using an analysis time between 30 and 60 s.

LA-ICP-MS analyses on individual fluid inclusions in samples of quartz, fluorite, and rhodochrosite were performed at ETH Zürich. The system consists of a 193 nm ArF Excimer laser (Lambda Physik, Germany) with an energy-homogenized (Microlas, Germany) beam profile (Günther et al. 1998) coupled with an ELAN6100 ICP quadrupole mass spectrometer (Perkin-Elmer, Canada). The laser system is characterized by a laterally homogeneous energy distribution, allowing depth-controlled ablation at a rate of 0.1–0.2 μm/shot, depending on laser energy and matrix chemistry. The resulting ablation craters are flat-bottomed and slightly conical. The optical imaging system permits the use of different pit diameters (8–100 μm) at constant energy density on the sample, by adjusting an aperture in the laser beam path. Simultaneous monitoring of the ablation process by optical microscopy and as real-time signal intensity is essential for controlled ablation of fluid inclusions. The sample was loaded along with the NIST SRM 610 glass standard into a 1 cm^3 ablation cell mounted on the stage of a modified petrographic microscope. Laser ablation aerosol was carried to the ICP-MS by a mixed He–Ar carrier gas. Analyses were performed in sequence, and each ablation was stored individually as a transient (i.e., time resolved) signal acquired in peak-hopping mode. Two analyses on the external standard at the beginning and the end of each set, required for offline data reduction, bracketed up to 16 analyses of unknowns. The certified glass standard SRM 610 was used as the external standard to calibrate analyte sensitivities, and bracketing standardization provided a linear drift correction. The analytical setup was tuned for optimum performance across the entire mass range and operated at conditions similar to those reported in Pettke et al. (2004). The data reduction scheme for fluid inclusions including criteria employed for the calculation of limits of detection is explained in detail in Heinrich et al. (2003).

Carbon dioxide was extracted from carbonate minerals by reaction with phosphoric acid at 72°C. Isotope ratios were measured using a ThermoFinnigan Delta Plus mass spectrometer operated by a Gasbench 2 in continuous He flow mode. For phosphoric acid, a fractionation factor α of 1.00812 was used for rhodochrosite (Böttcher 1993) and 1.00864 for calcite. The isotope values are expressed as δ values relative to VSMOW for oxygen and VPDB for carbon. The precision and accuracy is estimated at ±0.1‰.

Pure sulfide minerals were intimately mixed with V_2O_5 and measured directly on-line for their sulfur isotopic composition using an Elemental Analyzer connected to a ThermoFinnigan Delta Plus mass spectrometer. Results are expressed in the standard delta notation as permil difference to the VCDT standard. Reproducibility was better than 0.3‰. Isotope measurements were performed at the Geologisch-Paläontologisches Institut, Westfälische Wilhelms-Universität Münster.

Samples of fluorite from the early quartz–molybdenite–pyrite–topaz–muscovite–fluorite mineralization and main sulfide stage and rhodochrosite were finely ground in an agate mortar for analysis of REE by solution ICPMS. The analytical procedure is described in detail elsewhere (Dulski 2001). About 0.1 g of fluorite powder was dissolved using mixed acid digestion HF/HNO_3 under pressure and finally brought to 50 ml volume with 0.5 mol l^{-1} HCl (dilution factor 500). Rhodochrosite powder was dissolved in HNO_3. Ru and Re were added to aliquots of the solutions as internal standards for drift correction prior to analysis. Depending on the REE concentration of individual samples, the mixtures were diluted by a factor of 10 or 2. ICP-MS measurements were performed using an ELAN 5000A quadrupole mass spectrometer (Perkin-Elmer/SCIEX, Canada).

The distribution of REE and yttrium (REY) are illustrated by $REY_{C\text{-}1}$ patterns ($_{C\text{-}1}$: normalized to chondrite from Evensen et al. 1978) where Y is inserted between Dy and Ho according to its ionic radius (for details see Bau and Dulski 1995, and Bau 1996).

Galena and apatite were dissolved in 7 N HNO_3, fluorite was dissolved in concentrated H_2SO_4, and rhodochrosite was dissolved in 40% HF. After dissolution, samples were taken up in HCl or mixtures of H_2SO_4 and HCl. Rhodochrosite Pb was separated using an HCl–HBr ion-exchange chemistry (for a detailed description see Romer et al. 2005), galena Pb was loaded without additional chemical purification. Lead was loaded together with H_3PO_4 and silica-gel on single Re-filaments. Its isotopic composition was determined at 1200–1250°C on a Finnigan MAT262 multicollector thermal ionization mass spectrometer using static multicollection. Instrumental fractionation was corrected within 0.1%/a.m.u. as determined from repeated measurement of the lead isotope standard SRM 981. Accuracy and precision of reported Pb ratios are better than 0.1% at the 2-sigma level. Total procedural blanks for whole-rock samples are better than 15 pg Pb. Sr was separated using standard cation exchange techniques (Bio Rad AG50 W-X8, 100–200 mesh, 3.8 ml resin volume) in 2.5 N HCl medium. It was loaded on single Ta-filaments and its isotopic composition was determined on a VG Sector 54–30 multicollector thermal ionization mass spectrometer using a triple-jump dynamic-multicollection setup. $^{87}Sr/^{86}Sr$ data are normalized to $^{86}Sr/^{88}Sr=0.1194$. Repeated measurement of Sr standard NBS 987 during the measurement period gave 0.710249± 0.000010 (2σ, $n=8$). Analytical uncertainties of the individual measurements are reported as $2\sigma_m$. Total procedural blanks are less than 50 pg Sr.

Results

Fluid inclusion studies

Fluid inclusions were studied in both gangue and ore minerals, including quartz, fluorite, hübnerite, sphalerite, tetrahedrite, and rhodochrosite from all mineralization stages. Selection of fluid inclusions followed procedures outlined by Goldstein and Reynolds (1994) to identify fluid inclusion assemblages (i.e., coevally entrapped fluid inclusions along a geometric feature such as crystal planes, growth zones or healed microfractures). The studied samples were collected from all parts of the mine (Fig. 3). Bulk salinity of aqueous inclusions, expressed as equivalent wt.% NaCl, was calculated using the equation from Bodnar (1993). The composition of CO_2-bearing inclusions was calculated via ice and clathrate melting temperatures using the equations and diagrams from Barton and Chou (1993) and Bakker et al. (1996).

Fluid inclusion petrography

Many of the studied fluid inclusions are of primary origin using the criteria of Roedder (1984) and Goldstein and Reynolds (1994). However, in the earliest milky quartz I, it was impossible to determine the temporal classification for fluid inclusions owing to the large number of fluid inclusions along healed microfractures and in clusters where the inclusions are randomly distributed. At the Sweet Home Mine, four types of fluid inclusions have been characterized. These are, in decreasing order of abundance: aqueous, low-carbonic, liquid-rich inclusions (type 2); aqueous, liquid-rich two-phase inclusions (type 3); aqueous, carbonic inclusions with highly variable CO_2 content (type 1); and aqueous, low-nitrogen liquid-rich inclusions (type 4). It is conspicuous that none of the studied samples contain fluid inclusions with halite daughter minerals that have been described for the Climax orebodies (Hall et al. 1974) and other Climax-type deposits, notably Henderson and Questa (White et al. 1981; Cline and Bodnar 1994; Cline and Vanko 1995; Seedorff and Einaudi 2004b; Klemm et al. 2008). Vapor-rich inclusions without readily detectable CO_2 that commonly occur in porphyry copper deposits along with the halite-bearing inclusions are also not found in any sample studied.

Type 1 inclusions are restricted to the early milky, mica-bearing quartz where they occur in three-dimensional clusters in close proximity to type 2 and/or type 3 inclusions (Fig. 4a,b). Type 2 inclusions are the most common type in minerals from the early stage and from the main sulfide stage and are abundant in euhedral quartz, fluorite and gemmy rhodochrosite (Fig. 4c,d,h). Type 2 and type 3 inclusions are also rarely found in sphalerite and tetrahedrite (Fig. 4f,g). Late stage minerals, i.e., in pinkish (pale) rhodochrosite and fluorite that is grown on rhodochrosite contain only type 3 inclusions. Hübnerite either hosts type 3 or type 4 inclusions (Fig. 4e).

Fluid inclusion microthermometry

Microthermometric results of fluid inclusions in ore and gangue minerals are summarized in Table 1. Aqueous-carbonic type 1 fluid inclusions (Fig. 4a,b) in milky quartz from the early mineralization stage show variable salinity ranging between 7.5 and 12.5 wt.% equivalent NaCl and either V→L or, mostly, L→V homogenization of the carbonic phase at temperatures mostly between 29 and 31°C. Total homogenization temperatures (L+V→L) of about 350°C were observed for a few inclusions that show L→V homogenization of the carbonic phase, but complete homogenization was not achieved in gas-rich inclusions even when heated to 600°C.

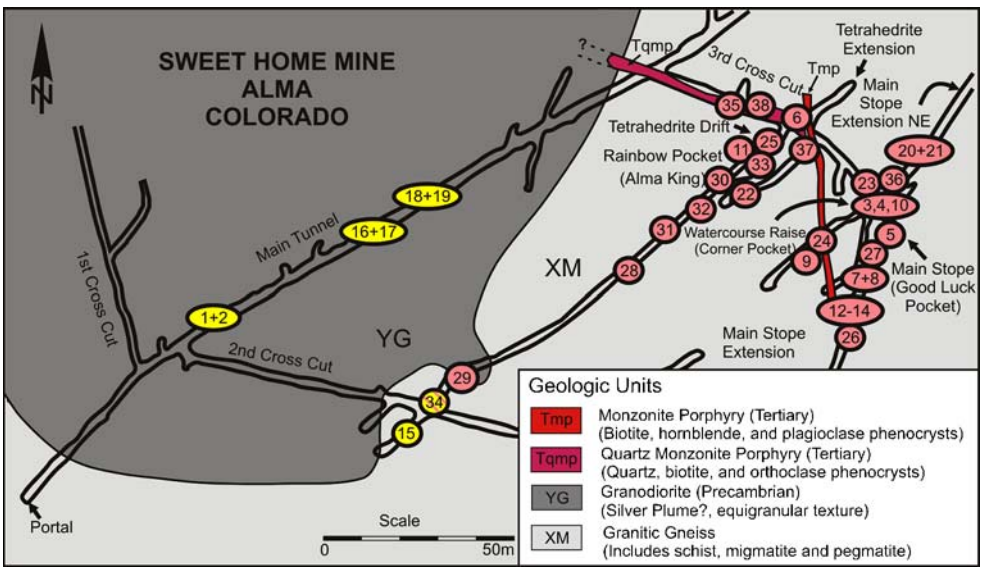

Fig. 3 Simplified geological map of the Sweet Home Mine (modified after Misantoni et al. 1998) showing sample sites. Sample suites marked in *yellow* exclusively contain minerals of the early stage; sample suites in *pink* may contain minerals from the early stage and from the main sulfide stage or only minerals from the main sulfide stage. Hübnerite may occur in samples marked in pink. *Numbers in yellow and pink fields* refer to analyzed samples in tables and figures. Sample fields showing more than one number identify different samples from the same locality

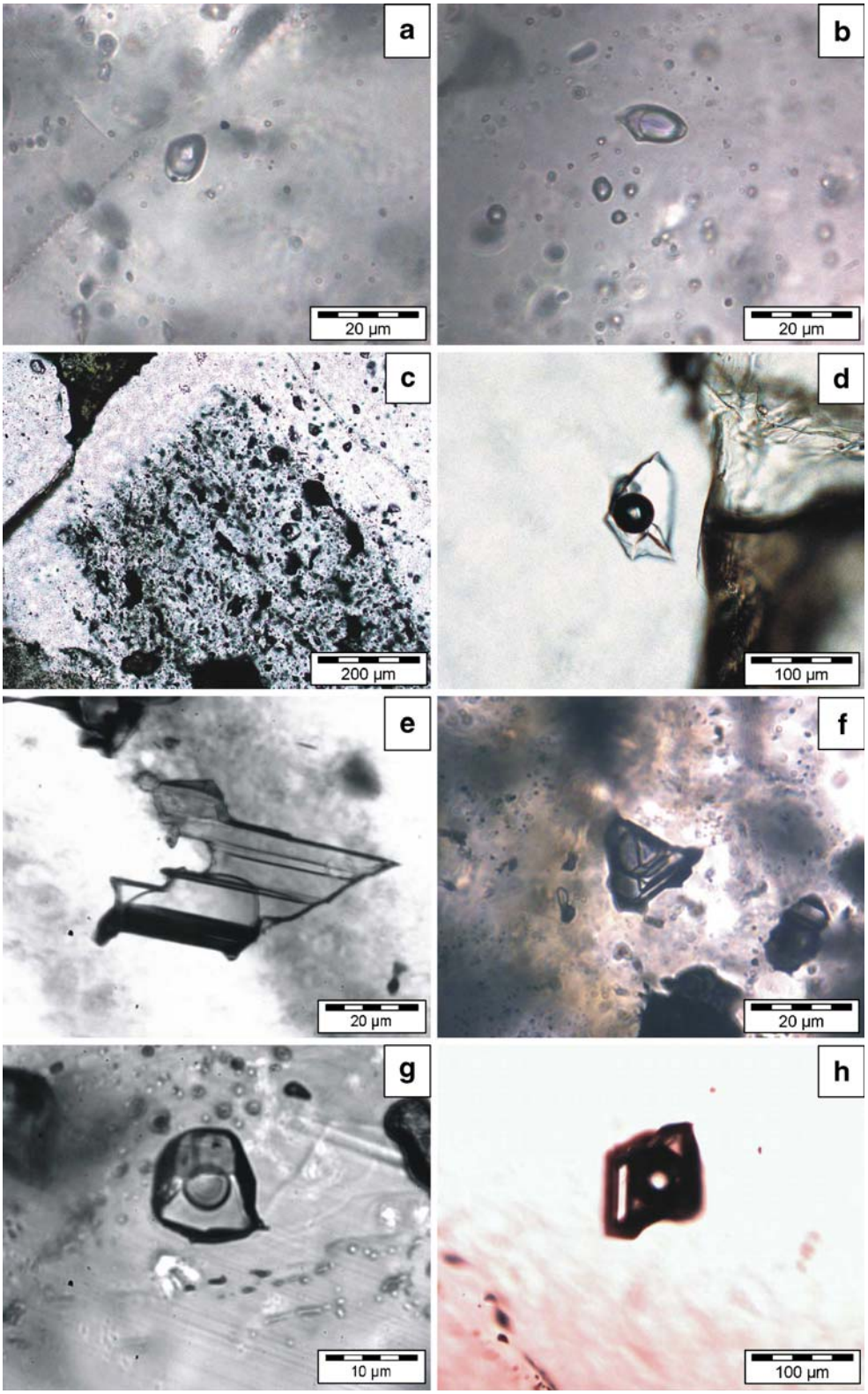

Fig. 4 Photomicrographs of fluid inclusions in early-stage quartz and fluorite. **a** Liquid CO_2-rich type 1 fluid inclusion in milky quartz. Homogenization into the liquid phase occurs at 30.1°C. **b** Vapor CO_2-rich type 1 fluid inclusions in milky quartz. Homogenization into the vapor phase occurs at 29.7°C. **c** Growth zone with liquid-rich, low-carbonic type 2 inclusions in euhedral quartz. **d** Isolated, primary type 2 inclusions in fluorite growing on quartz. Photomicrographs of fluid inclusions hosted in hübnerite and minerals from the main sulfide stage. **e** Infrared image of primary type 3 inclusion in hübnerite. **f** Primary type 2 inclusion in sphalerite photographed in white light. **g** Infrared image of a type 3 inclusion in tetrahedrite. **h** Primary type 3 inclusion in rhodochrosite photographed in white light

Type 1 inclusions are analogues to type II inclusions in quartz from the nearby giant Climax deposit (Hall et al. 1974).

The salinity of type 2 fluid inclusions (Fig. 4c) in euhedral early-stage quartz and fluorite is somewhat lower and varies between 5.5 and 7.8 wt.% NaCl equiv. (Table 1). Type 2 inclusions in euhedral quartz and early fluorite show melting of solid CO_2 recognizable only through cycling (Goldstein and Reynolds 1994), although a liquid carbonic phase is not

Table 1 Summary of microthermometric data of fluid inclusions hosted in various minerals from the Sweet Home Mine

Sample	Mineral	F.I. type	Tm Car	Tfm	Salinity	Th CO_2	Th
Early stage							
31	Quartz	1	−56.7 to −56.6 (15)	−16.5 to −12.8 (9)	7.5–12.5 (8)	30.3–30.8 (8)	313–365.4 (11)
31	Quartz	2	*n.o.*	−14 to −12.5 (12)	5.8–6.4 (14)	25.1–30.6 (18)	301.3–349 (26)
26	Quartz	2	−57.1 to −56.8 (6)	−14.5 to −12.5 (7)	2.8–9.5 (10)	*n.o.*	321.7–359.2 (10)
27	Quartz	2	−56.9 to −56.6 (15)	−14.3 to −11.9 (21)	5.4–6.9 (21)	*n.o.*	298.3–359.8 (24)
18	Fluorite	2	−57.2 to −57 (17)	−10.8 to −10 (7)	2.1–2.6 (17)	*n.o.*	334.1–335.8 (17)
Hübnerite stage							
26	Hübnerite	3	*n.o.*	*n.o.*	5.7–6.3 (9)	*n.o.*	325–355.6 (12)
30	Hübnerite	4	*n.o.*	*n.o.*	*n.o.*	*n.o.*	346.5–352.1 (8)
Main sulfide stage							
26	Sphalerite	2, 3	*n.o.*	−14 to −13.2 (5)	4–5.5 (8)	*n.o.*	217.5*–338 (8)
26	Sphalerite	2, 3	*n.o.*	−13.6 to −13.1 (6)	4–5.3 (9)	*n.o.*	238*–326 (9)
24	Tetrahedrite	3	*n.o.*	*n.o.*	7.2–7.9 (3)	*n.o.*	258–268.4 (5)
27	Rhodochrosite	2, 3	*n.o.*	−11 to −10.5 (4)	4.3–4.7 (4)	*n.o.*	264.3–283.4 (4)
25	Rhodochrosite	3	*n.o.*	*n.o.*	6.7–6.9 (4)	*n.o.*	259.4–264.2 (4)
7	Rhodochrosite	2	*n.o.*	−11.2 (1)	3.7–6.2 (7)	*n.o.*	280.9–289.2 (7)
30	Rhodochrosite	2, 3	*n.o.*	−11.7 to −11.1 (6)	3.2–4.4 (9)	*n.o.*	285.3–295.6 (4)
24	Rhodochrosite	3	*n.o.*	−11.5 (2)	5.6–5.9 (2)	*n.o.*	283.9–285.6 (3)
4	Rhodochrosite	3	*n.o.*	−116 to −11.4 (3)	4–4.3 (3)	*n.o.*	275.4–280.1 (3)
4	Fluorite	3	*n.o.*	−10.3 to −9.1 (10)	1.4–2.1 (18)	*n.o.*	179.2–191.3 (18)
30	Fluorite	3	*n.o.*	−9.2 to −8 (12)	0.7–1.4 (22)	*n.o.*	139.4–154.2 (22)

Numbers in parentheses refer to number of measurements. Salinity is reported in wt% NaCl equiv. (for details see text). Type 2 inclusions were identified by clathrate melting or laser-Raman spectroscopy. Type 2 inclusions in Sphalerite marked by * decrepitated prior to homogenization. Sample numbers refer to Fig. 3 *Tfm* first melting temperature, *n.o.* not observed

visible at room temperature. Clathrates melt between 5 and 9°C, indicating CO_2 content between 2.1 and 2.8 mol% (Barton and Chou 1993). Most homogenization temperatures of type 2 fluid inclusions from the early mineralization stage are above 300°C (Fig. 5). Type 2 inclusions were also measured in some samples of sphalerite and rhodochrosite (Table 2) and show higher salinity and homogenization temperatures when compared with type 3 inclusions (Table 2). Aqueous two-phase type 3 inclusions typically have salinity below 4.5 wt.% NaCl and show homogenization temperatures below 280°C. Salinity as well as homogenization temperatures of type 3 inclusions decrease continuously towards the end of the sulfide stage. These results are in good agreement with previous studies of fluid

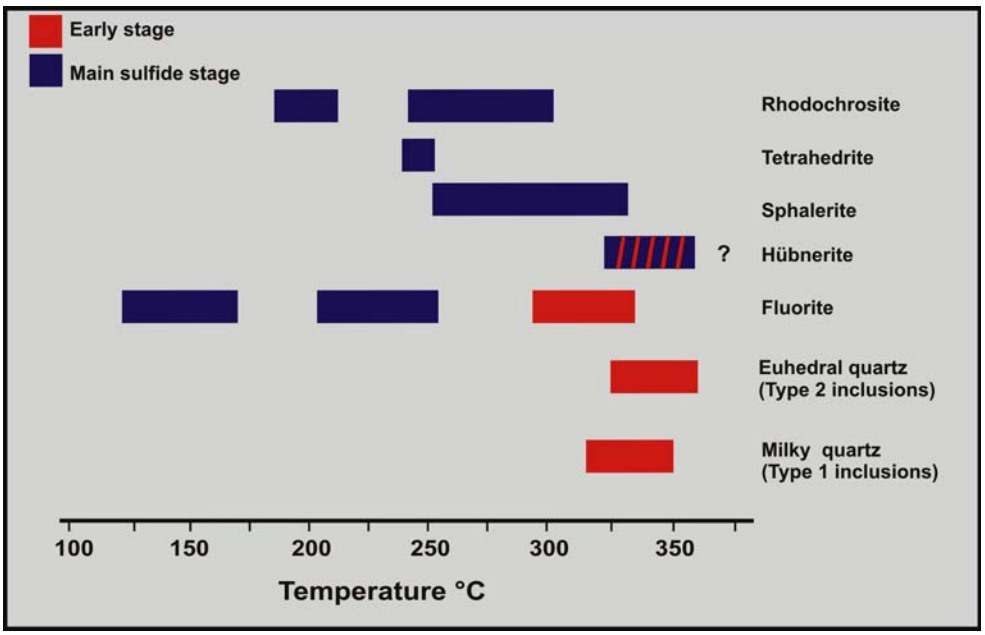

Fig. 5 Ranges of homogenization temperatures of fluid inclusions in various minerals from the early stage and main sulfide stage

Table 2 LA-ICPMS data of fluid inclusions in fluorite and quartz from the early mineralization stage and in rhodochrosite from the main sulfide stage; all values in microgram per gram

Sample	FI type	NaCl eq.[a]	Li	B	Na	Al	P	K	Ca	Mn	Fe	Cu	Zn	As	Rb	Sr	Mo	Cs	W	Pb	Ag
Rhodo 27	2	4.5	192	<275	15900	855	<802	4830	<21900	n.a.	<1540	<21	<90	<90	228	16	<24	107	<7	101	<11
Rhodo 27[b]	*2*	*4.3*	*367*	*308*	*14900*	*519*	*68*	*5280*	*1480*	*n.a.*	*4750*	*77200*	*20700*	*13500*	*132*	*3*	*<0.4*	*65*	*<0.2*	*23*	*1964*
Rhodo 27[c]	*2*	*4.7*	*288*	*524*	*16900*	*866*	*451*	*4200*	*<7350*	*n.a.*	*<2530*	*533*	*2630*	*121*	*123*	*19*	*1900*	*56*	*n.a.*	*n.a.*	*19*
Rhodo 27	2	4.5	168	152	16300	295	<74	3840	<1740	n.a.	850	6	43	33	109	5	<2	42	<0.7	1.4	<0.7
Rhodo 7	2	5.3	324	456	18600	144	<14	6090	<326	n.a.	<35	<0.5	<2	16	168	<0.1	<0.4	88	27	15	1
Rhodo 7	2	3.9	356	330	13900	316	<55	3780	<1270	n.a.	<103	55	<5	40	107	5	<1.2	53	15	30	9
Rhodo 7	2	3.9	265	271	13600	307	<146	4540	<3770	n.a.	1880	<10	<16	38	109	7	40	77	13	11	<1
Rhodo 7	2	3.8	327	85	13700	627	164	3400	6370	n.a.	8630	38	<14	44	129	41	10	64	44	41	16
Rhodo 7	2	3.8	204	228	13600	590	<67	3680	<1780	n.a.	<123	18	<8	22	162	6	<1.4	53	1.6	30	<0.6
Rhodo 7	2	3.8	196	267	12300	221	<76	4820	<1850	n.a.	1880	4	114	18	139	14	23	72	5	10	8
Rhodo 7	2	3.7	267	292	11800	323	336	4400	11300	n.a.	2450	130	521	84	173	16	120	102	14	42	16
Rhodo 7	2	3.9	261	505	13500	695	<205	4970	10300	n.a.	<386	139	354	39	142	7	102	67	58	46	25
Rhodo 25[c]	3	6.8	943	847	23800	290	<445	7890	<13100	n.a.	<964	<32	612	<47	198	19	281	91	<11	60	10
Rhodo 25	3	6.8	402	1010	23500	40	<349	8710	<9620	n.a.	<622	23	<45	73	175	10	42	75	7	20	<3
Rhodo 25	3	6.7	477	882	23500	231	<73	7670	<1820	n.a.	<119	25	<6	29	231	13	<2	89	18	2.5	1
Rhodo 25	3	6.7	477	695	23400	<37	<395	7790	<9310	n.a.	<652	77	361	<49	195	11	<12	89	13	25	8
Rhodo 25	3	6.9	655	1180	24450	681	486	7190	<1470	n.a.	<131	268	307	44	228	15	35	137	42	52	13
Rhodo 25	3	6.7	445	350	23500	133	<68	7500	<1850	n.a.	<150	41	194	30	197	13	<1.1	99	22	8	2
Fluorite 18	2	2.5	190	224	8750	1600	146	2890	n.a.	1000	346	82	128	42	87	392	8	45	25	56	27
Fluorite 18	2	2.4	119	275	7950	100	<16	3980	n.a.	766	73	25	24	12	155	111	1.1	71	2.2	9	2
Fluorite 18	2	2.1	125	176	7160	722	19	2930	n.a.	1380	101	13	28	12	121	152	1.7	56	2.2	16	3
Fluorite 18	2	2.2	190	<257	7590	<88	<605	2840	n.a.	<40	<1110	<26	<80	<86	45	<4	<12	18	<4	32	37
Fluorite 18	2	2.5	118	274	8230	204	492	4278	n.a.	594	<59	28	45	13	136	<0.2	<1.4	77	1.3	12	<0.8
Fluorite 18	2	2.2	72	294	7810	269	426	2252	n.a.	<22	<637	64	277	<43	50	45	<6	20	<3	9	<10
Quartz 31	2	6.0	<10	511	20700	<42	<358	7780	<7360	346	<648	61	<27	<44	217	5	<8	96	<3	9	<3
Quartz 31	2	6.0	88	487	20900	2080	<417	7260	<9790	553	<767	177	136	<41	326	4	<7	126	6	16	<2
Quartz 31	2	6.0	<2	407	21100	<16	<150	6750	<3050	977	<252	298	313	48	202	4	4	68	8	89	<1
Quartz 31	2	6.0	<12	206	21100	429	<475	6610	<11500	820	<734	426	117	65	157	5	<11	55	<6	89	<7
Quartz 31	2	6.0	123	423	20800	3680	<254	7570	<5530	970	<417	343	332	45	203	7	<5	88	4	92	3
Quartz 31	2	6.0	604	428	21000	8580	<134	7040	<3510	961	<261	449	165	74	201	5	1<4	78	<0.9	73	<0.9
Quartz 31	2	6.4	42	373	22400	613	440	7340	<3340	475	413	29	36	<18	238	5	<3.4	73	3	10	2
Quartz 31	2	6.1	265	311	21300	4740	81	7120	<716	371	<46	38	17	<5	215	3	<1.0	63	0.5	5	<0.3
Quartz 31	2	5.8	31	489	20000	480	246	7500	<2380	422	<182	536	57	40	229	2	0.5	79	<1.6	36	<1
Quartz 31	1	7.6	135	<332	27300	340	<910	7010	17700	<70	13800	1540	<67	<93	95	76	<14	29	<8	45	<8
Quartz 31	1	7.6	122	354	27100	2010	<551	7580	<10700	5960	1170	3850	573	<52	232	21	<12	60	<6	39	<9
Quartz 31	1	10.5	134	343	37600	1710	<701	9900	<14100	1990	32500	3480	740	<72	350	22	<11	89	<6	506	58
Quartz 31	1	10.5	56	647	37100	9190	<1350	11200	<25300	108	<1970	280	<119	<124	84	81	<22	29	<12	<20	<9
Quartz 31	1	11.0	84	<173	39200	1600	550	10900	<9590	70	<859	50	136	<47	82	92	<18	51	<5	36	<10
Quartz 31	1	10.5	83	445	36300	7630	<926	13400	<17100	1710	<1240	126	111	<98	347	25	<26	71	<8	65	<6
Quartz 31	1	10.5	217	<515	37100	<222	<1900	11100	<41100	1660	<3420	482	194	<185	217	14	<31	99	<17	143	<21
Quartz 31	1	10.4	145	<317	37400	<130	<869	9440	<18100	83	<1510	<68	<73	<83	103	91	<23	60	<9	<13	<15
Quartz 31[d]	*1*	*10.5*	*<57*	*<362*	*38200*	*2950*	*<1440*	*8410*	*763000*	*20100*	*3970*	*<62*	*163*	*<152*	*108*	*1200*	*<40*	*46*	*<12*	*84*	*<18*
Quartz 31	1	10.3	<84	<463	36900	<425	<2470	9530	<46100	2160	<3980	<131	543	<341	291	19	<103	56	<52	89	<46
Quartz 31	1	10.3	434	349	36900	<117	<776	9600	<15700	3560	4010	1720	280	<90	254	33	<25	75	<8	106	13
Quartz 31	1	10.3	240	370	36200	1650	<642	1160	28200	6920	3070	3720	234	<9	294	88	<29	86	48	109	11
Quartz 31	1	10.3	122	<159	36100	<88	<545	1180	<12000	57	<1060	196	<74	<65	82	135	<22	51	11	24	9
Quartz 31	1	10.3	55	309	34500	1150	<241	16000	<4980	2360	<371	963	77	52	509	11	4	109	20	14	<2
Quartz 31	1	10.3	93	<760	36200	<266	<2000	11600	<37500	582	<3080	5030	<258	<218	392	<8	<56	117	<36	60	<25
Quartz 31	1	10.3	14	228	36400	3460	<434	10900	<8340	1140	<660	1150	63.6	<55	354	9	<14	102	12	30	<3
Quartz 26	2	6.5	49	<288	23100	<98	<886	6540	<16700	608	<927	41	99	<87	252	12	24	104	<18	13	<12
Quartz 26	2	6.5	<12	287	22800	<62	466	7460	<9340	809	<938	27	<46	61	299	7	<11	122	<49	18	<7

Quartz 26	2	6.5	30	611	22500	<64	384	8070	<1160	574	<760	125	225	62	307	10	20	123	34	20	<4
Quartz 26	2	6.5	<28	629	22600	<109	777	7960	<17200	701	<1370	<40	<89	<101	304	<4	<13	122	11	<13	<9
Quartz 26	2	6.0	<6	578	20600	1930	384	7930	<4790	978	318	372	324	44	310	3	<5	124	26	37	4
Quartz 26	2	5.2	<4	553	18100	98	355	6360	<5080	385	<463	71	<23	<26	246	2	<7	90	6	9	<3
Quartz 26	2	6.6	<8	392	22500	777	<312	9130	<7080	351	<469	<14	<36	32	328	7	<5	129	<2	7	<2
Quartz 26	2	6.7	<18	<220	23600	<120	<882	7480	<18800	310	<1270	<44	<68	<84	329	2	<14	109	<13	<11	<11
Quartz 26	2	6.5	<14	<294	23200	<127	<948	6440	<19000	493	<1530	<31	172	<110	316	<4	<28	159	14	38	<6
Quartz 26	2	9.0	<10	682	31000	<51	703	11900	<8870	361	<713	407	<37	<37	432	4	<10	202	<4	10	<5
Quartz 26	2	9.5	<21	579	32300	<118	<986	13400	<17300	1390	<1380	555	149	<122	391	10	<17	188	<9	97	<9
Quartz 26	2	6.5	<9	486	22800	<52	499	7470	<6120	429	<495	651	142	37	281	3	<10	117	22	21	<3
Quartz 26	2	4.7	<7	371	16500	<37	489	5240	<6510	937	<483	2140	330	37	207	<2.0	<5	90	6	112	<3
Quartz 26	2	2.4	255[c]	233	8450	8260	<459	2660	<8940	716	<809	1950	97	<4	90	<2.3	<7	53	<4	72	<17

Data set in italics are inclusions contaminated by accidentally trapped solids, e.g., carbonates or sulfides, and are therefore discarded from further discussion. For values below the limit of detection, the detection limit is given as "<value"(calculated as 3 standard deviations of the background divided by sensitivity). *n.a.* not available (signals dominated by host mineral). Sample numbers refer to Fig. 3.

[a] In weight percentage calculated after Bodnar (1993)

[b] Interpreted to result from accidentally trapped sulfosalt inclusion

[c] Interpreted to result from accidentally trapped solid inclusion

[d] Interpreted to result from accidentally trapped carbonate inclusion

inclusions in gangue minerals from the Sweet Home Mine (Reynolds 1998).

Type 4 inclusions in hübnerite (Fig. 4e) show final ice melting around −5°C and melting of clathrate between 3.6 and 3.8°C. Raman spectroscopic analyses show the presence of nitrogen in these inclusions. Other samples of hübnerite host type 3 inclusions with salinities between 5.7 and 6.3 wt% equivalent NaCl. The total homogenization temperatures of both nitrogen-bearing and aqueous inclusions in hübnerite are between 325 and 356°C (Table 1). Other ore and gangue minerals (including rhodochrosite) from the main sulfide stage host either type 2 or type 3 inclusions. The latter mostly occur in minerals that precipitated at lower temperatures towards the end of the main sulfide stage, as indicated by the homogenization temperatures of fluid inclusions (Table 1 and Fig. 5).

In summary, temperatures, salinities and CO_2 contents of the fluid inclusions decrease with time, with a sharp break in CO_2 content at about 250°C.

P–T conditions of fluid entrapment in quartz

Most early milky quartz veins at the Sweet Home Mine are massive banded veins without open space textures common in shallow environments. This contrasts markedly with the vuggy nature of the later stages containing material prized by mineral collectors. We interpret these textures as being indicative of different pressures during formation: higher pressures, perhaps near lithostatic existed during the formation of early quartz and hydrostatic pressure probably existed during filling of the vugs.

Type 1 inclusions are only hosted in the early milky quartz. These inclusions may be interpreted to represent mixtures of immiscible fluids that formed when an originally homogeneous fluid intersected the solvus during cooling or decompression (Diamond 1994). The relatively narrow range in compositions of these inclusions suggests that, if immiscibility occurred, the *P–T* fluid path must have intersected the solvus near its crest, where the compositions of the two immiscible phases are not significantly different. The fact that vapor-rich type I inclusions do not homogenize, even when heated to 600°C, is consistent with trapping mixtures of two fluids beneath the solvus (Bodnar et al. 1985). Alternatively, type 1 inclusions may have been trapped under a fluctuating pressure regime or may represent heterogeneous mixtures of two fluids of diverse origin.

It is possible to estimate the trapping conditions based on the temperature and mode of homogenization of the CO_2 liquid and vapor phases in the inclusions. There is a systematic relationship between these parameters and the PTX trapping conditions that is defined by the PVTX properties of the system H_2O–CO_2 (Bodnar et al. 1985). Most of the CO_2-bearing inclusions in the early, milky quartz

show homogenization temperatures of about 25–31°C, some homogenize to the liquid phase and some to the vapor phase. Assuming a trapping temperature of 400°C, the inclusions must contain between about 5–40 mol% CO_2 and must have been trapped at pressures from about 0.7–3 kbars (Fig. 6). The large majority of the inclusions homogenize in the range from about 29–31°C, corresponding to about 20–30 mole% CO_2 and trapping pressures of about 0.8–1.5 kbars (blue shaded area, Fig. 6). Inclusions trapped at PTX conditions outside of the area shown on Fig. 6 cannot show the temperatures and modes of homogenization of the inclusions in early, milky quartz. Considering a lithostatic pressure regime for the formation of early quartz, pressures of 0.8 to 1.5 kbars correspond to a depth of about 3 to 5.6 km. A lithostatic pressure regime seems to be plausible because early quartz only precipitated at the outer rims of voids that contain euhedral quartz crystals in the center. This might indicate that the formation of early milky quartz occurred contemporaneously with the opening of small voids which expanded continuously with movement along N–S and N–E trending faults (Misantoni et al. 1998). The phase transitions of type 1 inclusions either to the liquid or vapor phase seem to reflect a pressure regime that fluctuated from high to lower pressure. The fact that euhedral quartz crystals crystallized in open voids (note: there is a continuous transition from milky to euhedral quartz) indicates that the pressure regime dropped from lithostatic to hydrostatic under near open system pressure conditions.

Assuming that the Type 2 inclusions in euhedral quartz contain at least 2 mol% CO_2, this would require a minimum pressure of about 300 bars, or 3 km depth at hydrostatic pressures. The depth would be shallower if the pressure regime was between hydrostatic and lithostatic (Roedder and Bodnar 1980).

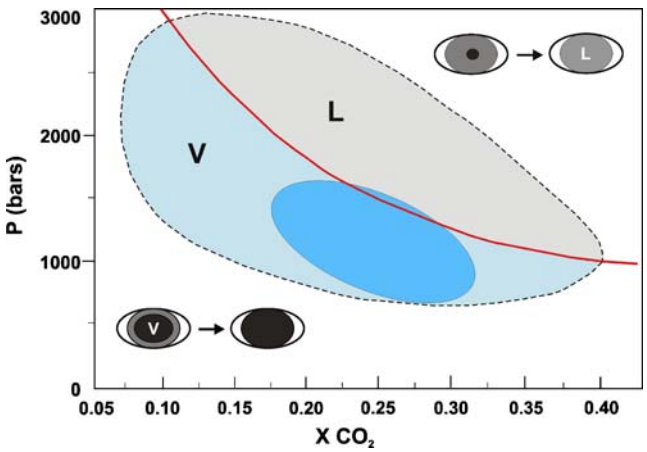

Fig. 6 Relationship between trapping pressure and XCO_2 for H_2O–CO_2 fluid inclusions trapped at 400°C, calculated using the algorithm in Bodnar et al. (1985). The lightly shaded areas labeled *L* and *V* represent the total P-XCO_2 area defined by inclusions in early milky quartz and the darker shaded region from about 20–30 mol% CO_2 and 1,000–1,500 bars corresponds to the majority of the inclusion measurements

Fluid inclusion composition

LA-ICPMS analyses were performed on individual fluid inclusions in quartz, fluorite and rhodochrosite to determine the elemental composition. The results of the LA-ICPMS analyses are given in Table 2. The fluids are dominated by Na and K but generally show low metal contents when compared with fluid inclusion data from porphyry–Cu–Au (Bodnar 1995; Landtwing et al. 2005) and other Climax-type deposits (Cline and Vanko 1995; Klemm et al. 2008). The Cu content in early quartz-hosted inclusions is similar to that of inclusions in quartz in barren granites in New Mexico (Audétat and Pettke 2003). However, fluid inclusions in quartz from the Sweet Home Mine show considerable concentrations of incompatible elements such as Cs and Rb (Table 2). The mean Rb/Cs ratios decrease from 3.3 for fluid inclusions in milky quartz to values of 2.4 in euhedral quartz and 2.2 and 2.1 in fluorite and rhodochrosite, respectively. Decreasing Rb/Cs ratios may indicate progressive fractionation of F-rich felsic melts (Thomas et al. 2005). At the Sweet Home Mine, type 1 fluid inclusions in early quartz show similar or lower K/Rb ratios but mostly higher Cs contents when compared to fluid inclusions hosted in quartz from the magmatic–hydrothermal breccia from Questa (Fig. 7). The Cs content of fluid inclusions hosted in early quartz is similar to that of stockwork quartz-hosted inclusions from the Questa Mo deposit but the K/Rb ratios are mostly lower (Fig. 7). Generally, with the exception of Cs, all analyzed inclusions in various minerals from the Sweet Home Mine show several times lower metal content when compared with fluid inclusions in quartz from Questa (Fig. 7).

REY distribution in fluorite

Fluorite samples from the early mineralization stage (samples 1 and 2) are characterized by significantly higher rare-earth-element and yttrium (REY) concentrations when compared with fluorite samples from the main sulfide stage (Fig. 8). However, all samples are strongly depleted in light REE (LREE) compared to the middle (MREE) and heavy REE (HREE). Early-stage fluorites as well as some fluorite samples from the main sulfide stage show small negative Eu anomalies. If the fluorite-forming fluids at the Sweet Home Mine had an igneous source, fluorites should show roughly chondritic Y/Ho ratios of 28 (Taylor and McLennan 1985), and REY patterns similar to their parent liquids or host rocks (Bau and Dulski 1995). Small negative Eu anomalies and Y/Ho ratios between 26 and 27 are only observed in the two fluorite samples from the early stage

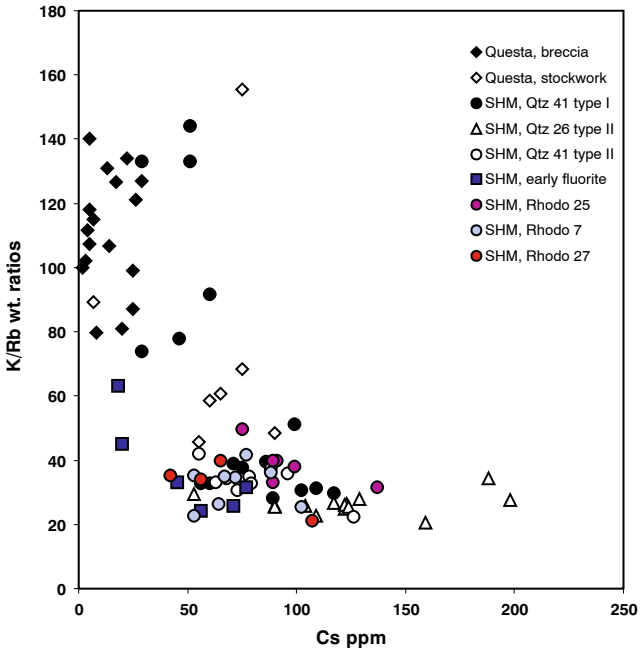

Fig. 7 Cs versus K/Rb diagram of analyzed fluid inclusions in quartz and fluorite from the early-stage mineralization of the Sweet Home Mine and quartz from the Questa, New Mexico, Mo deposit (Klemm 2006). Fluid inclusions in quartz from magmatic–hydrothermal breccia quartz (Questa) show the lowest Cs content. The increase of Cs content in quartz-hosted inclusions from younger Questa stockwork mineralization suggests that the ore-forming fluids were derived from a more fractionated magma (Klemm 2006). Type I inclusions in early milky quartz from the Sweet Home Mine show K/Rb and Cs content that show good agreement with the Questa data. At the Sweet Home Mine, the K/Rb ratios decrease and Cs content in fluid inclusions increases with progressive mineralization probably indicating that the fluids originated from a more fractionated source than at Questa

(Table 3). All fluorite samples from the main sulfide stage show higher Y/Ho ratios between 37 and 86 typical of medium-temperature, fluorite-forming hydrothermal systems (Bau and Dulski 1995). Therefore, it seems unlikely

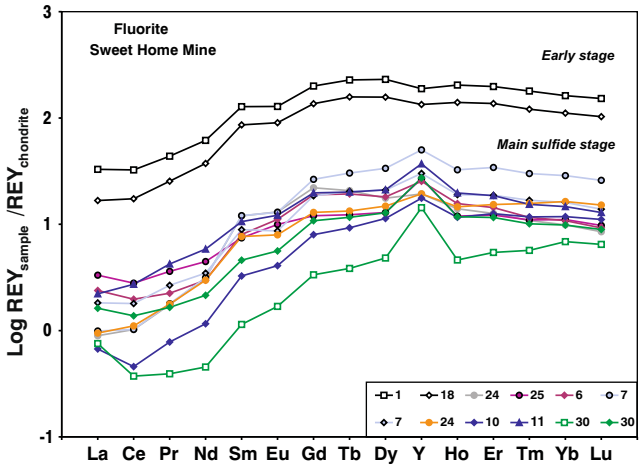

Fig. 8 REY distribution patterns of fluorite samples from the early stage and main sulfide stage

that the fluorite-forming fluids of the main sulfide stage are dominated by a nearby felsic magmatic source. Instead, positive Y-anomalies in the REY patterns of the younger fluorite samples suggest considerable large-scale fluid migration or the involvement of an additional fluid (Bau and Dulski 1995). Negative Eu anomalies are not necessarily indicative of a fluid origin from Eu-depleted felsic magmas (Lüders et al. 1993; Möller et al. 1998). Decoupling of Eu from its trivalent neighbors and the generation of negative Eu anomalies (this requires that some of the Eu occurs as Eu^{2+}) may also be indicative that fluorite precipitation occurred from fluids that have experienced temperatures >200°C (Bau and Möller 1992). For most of the Sweet Home Mine fluorite samples this inference is compatible with the fluid inclusion data (Fig. 5).

Isotope geochemistry

Carbon and oxygen isotopic composition of rhodochrosite

Rhodochrosite displays a wide range of $\delta^{18}O_{VSMOW}$ values ranging from −0.5 to +19.0‰ with most values scattering around 11±2‰ (Fig. 9). The variability in oxygen isotope values, which contrasts with data from the Creede and Sunnyside epithermal vein deposits, San Juan Mountains, Colorado (Casadevall and Ohmoto 1977; Bethke and Rye 1979), cannot be related to temperature variations (300 to 260°C) during rhodochrosite formation alone. The C–O isotopic trend is consistent with at least two isotopically distinct aqueous fluids during the formation of gem-quality rhodochrosite. Using the oxygen isotope fractionation equation between rhodochrosite and water from Böttcher (1993) and temperatures derived from our fluid inclusion study (~260 to 300°C), we can calculate the isotopic composition of fluids responsible for precipitating rhodochrosite. The isotopically heavy rhodochrosite ($\delta^{18}O_{rhodo}$= ~11±2‰) was formed from aqueous fluids with $\delta^{18}O_{water}$= ~+5‰. This dominating isotopically heavy fluid is most probably derived from a magmatic source, but could alternatively be a hydrothermal fluid of any origin that has fully equilibrated with silicate rocks at high temperatures (>400°C) and low water–rock ratios.

Some gem-quality rhodochrosite samples and some pale rims of isotopically heavy rhodochrosites have much lower oxygen isotope values of ~0 to +6‰. The isotopically lightest rhodochrosite ($\delta^{18}O_{rhodo}$=~0‰) was deposited from an aqueous fluid with $\delta^{18}O_{water}$ of −6‰ that suggests a meteoric water component. Rhodochrosite with intermediate isotope compositions (~+6‰) was most likely precipitated from a mixture of the two fluids.

Carbon isotope values of rhodochrosite (−8.5±0.6‰) are, in contrast to oxygen, rather uniform and indicate a single carbon source with a $\delta^{13}O_{CO2}$ of −8‰ using the

Table 3 Trace element concentrations for fluorite samples from the Sweet Home Mine (all concentrations in microgram per gram)

Sample	1	18	24	25	6	7	7	24	10	11	30	30
Rb	21.6	15.2	<0.3	1.07	14.2	<0.3	0.37	<0.3	<0.3	<0.3	<0.3	<0.3
Sr	558	413	61.7	141	72.5	203	138	160	198	123	189	89.5
Y	294	209	30.1	41.9	39.6	78.0	47.0	30.1	27.4	57.8	22.3	42.5
Zr	0.28	1.68	0.22	1.35	2.81	1.07	0.54	0.36	0.25	0.23	0.33	0.34
Cs	0.13	0.11	<0.02	0.03	0.11	<0.02	<0.02	<0.02	<0.02	<0.02	<0.02	<0.02
Ba	1.12	2.47	0.21	20.2	2.09	0.56	0.33	0.30	0.23	2.67	0.85	1.27
La	7.73	3.93	0.21	0.78	0.56	0.23	0.43	0.22	0.16	0.52	0.18	0.38
Ce	19.6	10.5	0.62	1.68	1.19	0.62	1.08	0.67	0.28	1.64	0.22	0.83
Pr	3.89	2.26	0.16	0.32	0.20	0.16	0.24	0.16	0.07	0.38	0.03	0.15
Nd	27.8	16.9	1.42	2.02	1.35	1.42	1.57	1.35	0.52	2.64	0.21	0.97
Sm	18.8	12.7	1.76	1.09	1.18	1.77	1.31	1.13	0.48	1.56	0.17	0.67
Eu	7.18	5.06	0.73	0.56	0.62	0.73	0.48	0.44	0.23	0.68	0.09	0.31
Gd	39.4	26.8	4.35	2.37	3.74	5.21	3.65	2.55	1.57	3.89	0.66	2.13
Tb	8.20	5.68	0.75	0.44	0.69	1.09	0.73	0.48	0.33	0.72	0.14	0.42
Dy	56.0	38.2	4.28	3.13	4.40	8.16	5.09	3.60	2.76	5.12	1.17	3.12
Ho	11.4	7.84	0.78	0.67	0.88	1.82	1.06	0.82	0.65	1.10	0.26	0.66
Er	31.4	21.8	2.01	1.94	2.28	5.44	2.98	2.44	2.00	2.96	0.86	1.84
Tm	4.30	2.90	0.26	0.26	0.28	0.72	0.40	0.38	0.28	0.37	0.14	0.24
Yb	26.5	18.1	1.61	1.81	1.76	4.68	2.61	2.67	1.92	2.39	1.12	1.60
Lu	3.66	2.47	0.20	0.23	0.22	0.62	0.33	0.36	0.27	0.31	0.16	0.21
Hf	<0.04	0.09	<0.04	0.07	0.14	<0.04	<0.04	<0.04	<0.04	<0.04	<0.04	<0.04
Pb	1.07	6.48	4.36	161	5.36	2.31	0.97	3.87	2.60	2.79	1.55	3.59
Th	13.0	9.00	0.25	0.30	0.42	2.67	11.83	0.40	0.12	0.25	0.04	0.11
U	0.02	0.04	0.11	0.16	0.11	<0.02	<0.02	0.20	<0.02	0.03	<0.02	<0.02
Y/Ho	25.8	26.7	38.6	62.5	45.0	42.9	44.3	36.7	42.2	52.5	85.8	64.4

Sample numbers refer to Fig. 3

fractionation equations of Böttcher (1993) and Deines (2004). This value is consistent with a magmatic source or an average mixed crustal source.

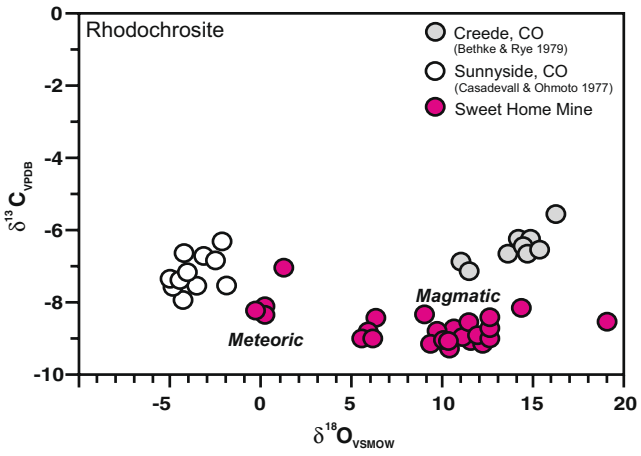

Fig. 9 Carbon and oxygen isotope compositions of rhodochrosite from the Sweet Home Mine. Isotope values of rhodochrosite from the Creede and Sunnyside vein deposits, San Juan Mountains, Colorado, are shown for comparison

Sulfur isotopes

Sulfur isotopes were measured in 29 sulfide samples from the early and main sulfide stage. The $\delta^{34}S$ values of the analyzed samples range from +1.7 to −4.2‰ (Table 4). Positive $\delta^{34}S$ values were only measured in pyrite from the early quartz–molybdenite–pyrite–topaz–muscovite–fluorite stage as well as in pyrite and some sphalerite samples from the main sulfide stage. Paragenetically, the latter are the first sulfides that were deposited during the main sulfide stage. Equilibrium fractionation estimated for coexisting sulfide pairs mostly gave unrealistic formation temperatures (Table 4) indicating that most of the sulfides studied were not deposited contemporaneously from the same fluid. Only four sulfide pairs gave realistic model temperatures in the temperature range between 260 and 340°C (Table 4). The $\delta^{34}S$ values of pyrite from the main sulfide stage are somewhat lighter (+1.6 to +0.9‰) than pyrite from the early stage (about +1.7‰) but the $\delta^{34}S$ values of sphalerite are highly variable (+1.2 to −2.8‰). Early black sphalerite samples show positive $\delta^{34}S$ values whereas brown sphalerite associated with younger sulfides shows negative $\delta^{34}S$ values. Positive mean $\delta^{34}S$ values of about 2‰ are reported from molybdenite and pyrite samples from all major porphyry Mo deposits in the COMB and are

Table 4 Sulfur isotopic composition of ore minerals from the early stage and the main sulfide stage (MSS)

Sample no.	Min. stage	Mineral	$\delta^{34}S$ [‰]	Model temperatures	
15	Early stage	Pyrite	+1.71		
12	Early stage	Pyrite	+1.73		
28	MSS	Chalcopyrite	−3.85	Chalcopyrite–pyrite	<<100°C
28	MSS	Pyrite	+0.95	Pyrite–sphalerite	>>500°C
28	MSS	Sphalerite	+0.66	Sphalerite–chalcopyrite	<<100°C
6	MSS	Sphalerite	+0.57		
24	MSS	Galena	−4.18		
26	MSS	Sphalerite	+0.7		
11	MSS	Galena	−0.13		
24	MSS	Tetrahedrite	−4.01		
29	MSS	Galena	−1.17		
24	MSS	Tetrahedrite	−3.73		
32	MSS	Galena	−2.08	Galena–sphalerite	>>500°C
32	MSS	Sphalerite	−2.52	Sphalerite–chalcopyrite	≈ 290°C
32	MSS	Chalcopyrite	−1.69	Chalcopyrite–galena	>>500°C
32	MSS	Sphalerite	−2.42		
33	MSS	Galena	−2.19	Galena–sphalerite	>>500°C
33	MSS	Tetrahedrite	−4.09		
34	Early stage?	Pyrite	+1.57	Pyrite–chalcopyrite	<<100°C
34	MSS	Chalcopyrite	−3.44		
35	MSS	Sphalerite	+1.09		
36	MSS	Chalcopyrite	−1.72	Chalcopyrite–sphalerite	≈ 260°C
36	MSS	Sphalerite	−2.82		
37	MSS	Sphalerite	+0.7	Sphalerite–pyrite	≈ 340°C
37	MSS	Pyrite	+1.34		
38	MSS	Galena	−1.64	Galena–chalcopyrite	>>500°C
38	MSS	Chalcopyrite	−1.93	Chalcopyrite–sphalerite	<<100°C
38	MSS	Tetrahedrite	−2.42		
38	MSS	Sphalerite	+1.24	Sphalerite–galena	≈ 280°C

interpreted to be of magmatic origin (Stein and Hannah 1985). Therefore, the positive $\delta^{34}S$ values of pyrite from the early stage and early main sulfide stage are interpreted to indicate a magmatic fluid component, reflecting the sulfur isotopic composition of the sulfur melt species (Ohmoto and Rye 1979). All other analyzed sulfide samples from the main sulfide stage show negative $\delta^{34}S$ values (Table 4). Sulfur isotopic fractionation in hydrothermal ore deposits is a function of temperature, pH, fO_2, isotopic composition of the ore-forming fluid, and/or the sulfur speciation in the fluid (Ohmoto and Rye 1979). Assuming a homogeneous fluid source, changes in fO_2 and/or pH would have been required to change the $\delta^{34}S$ values of the various sulfides during ore deposition at the Sweet Home Mine. However, large changes in fO_2 are unlikely, since this would have led to a significant increase of the sulfate content in the fluid (Ohmoto and Rye 1979) and the precipitation of sulfates during the main sulfide stage. A significant decrease in pH is also unlikely because this would have prevented the precipitation of rhodochrosite. Alternatively, the observed variation in the sulfur isotopic composition of pyrite, sphalerite, galena, and tetrahedrite can be interpreted in terms of different sulfur sources. Considering a sulfur source from a nearby magmatic intrusion for pyrite deposited during the early mineralization stage, the continuous decrease of the $\delta^{34}S$ values of sulfides that formed during the main sulfide stage can be explained by assimilation of sulfur from the country rocks or supply of sulfur-bearing externally derived fluids that interacted with the country rocks.

Lead isotope signatures of rhodochrosite and galena

The Pb isotopic composition of Tertiary mineralization and Tertiary magmatic rocks of the eastern Rocky Mountains is well known (e.g., compilations in Doe and Zartman 1979; Stein 1985; Kelley and Ludington 2002). Hydrothermal vein-type mineralization and granitoids related to porphyry-type Cu and Mo mineralization have similar Pb isotopic compositions that differ distinctly from mafic and alkaline mantle-derived volcanic rocks which generally have lower $^{208}Pb/^{204}Pb$ signatures at comparable $^{206}Pb/^{204}Pb$ values (Fig. 10). The Pb isotopic composition of rhodochrosite from the Sweet Home Mine (Table 5) is, at least for crystals belonging to the same mineralization stage, homogeneous and falls within the Pb field of COMB mineralization

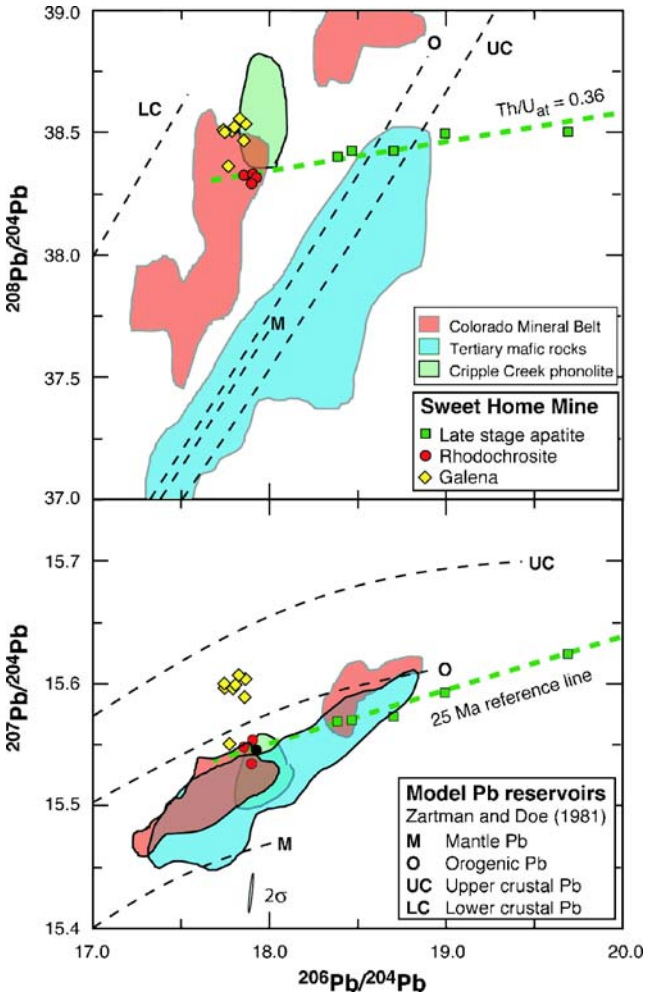

Fig. 10 $^{207}Pb/^{204}Pb$ vs. $^{206}Pb/^{204}Pb$ and $^{208}Pb/^{204}Pb$ vs. $^{206}Pb/^{204}Pb$ diagrams for galena, rhodochrosite, and apatite samples from the Sweet Home Mine. Pb-reference fields from Doe and Zartman (1979); Stein (1985); and Kelley and Ludington (2002). Pb growth curves from Zartman and Doe (1981)

(Fig. 10). The offset to higher $^{208}Pb/^{204}Pb$ values for deposits of the COMB may reflect assimilation of ancient lower continental crust (Zartman and Doe 1981; Stein 1985). The Pb isotopic composition of sulfide stage galena is slightly heterogeneous: seven samples cluster around $^{206}Pb/^{204}Pb \approx 17.8$, $^{207}Pb/^{204}Pb \approx 15.6$, and $^{208}Pb/^{204}Pb \approx 38.5$; one sample (04-09, Table 5) has markedly lower $^{207}Pb/^{204}Pb$ and $^{208}Pb/^{204}Pb$ values. This single galena sample shows the same Pb isotopic composition as the rhodochrosite samples (Table 5) and corresponds to the projected initial Pb isotopic composition of late-stage apatite (Romer and Lüders 2006). All analyzed galena samples belong to the main sulfide stage in which rhodochrosite, apatite and possibly the deviating galena sample were deposited late. Early galena samples differ in their Pb compositions from younger minerals (Fig. 10). This implies that the Pb in early and late fluids originated from different sources. The galena Pb is dominated by old crust with a relatively high time-integrated Th/U ratio. The shift of the Pb isotopic composition from high $^{207}Pb/^{204}Pb$ and $^{208}Pb/^{204}Pb$ values to low values indicates that the contribution of Pb from old crustal sources was much more prominent in the early main sulfide stage than during the subsequent rhodochrosite formation. The initial Pb isotopic composition of rhodochrosite and apatite falls into the field typical for COMB mineralization (Fig. 10). Thus, the Pb isotopic composition of galena, rhodochrosite, and apatite provides evidence for the involvement of at least two lead sources in the formation of main sulfide mineralization at the Sweet Home Mine.

Initial $^{87}Sr/^{86}Sr$ of fluorite, rhodochrosite, and apatite

The initial $^{87}Sr/^{86}Sr$ ratio was determined on fluorite from the early stage as well as from the main sulfide stage, and on rhodochrosite and apatite precipitated on rhodochrosite

Table 5 Lead isotope composition of minerals from the Sweet Home Mine, Colorado, U.S.A.

Sample[a]	Pb [ppm]	U [ppm]	$\frac{^{206}Pb^b}{^{204}Pb}$	$\frac{^{207}Pb^b}{^{204}Pb}$	$\frac{^{208}Pb^b}{^{204}Pb}$	$\frac{^{238}U^b}{^{204}Pb}$
Galena						
11 a			17.866	15.604	38.543	
29 a			17.743	15.597	38.506	
39			17.789	15.597	38.511	
25			17.804	15.600	38.511	
33			17.771	15.552	38.373	
24			17.826	15.607	38.559	
11 b			17.859	15.589	38.475	
29 b			17.741	15.599	38.521	
Rhodochrosite						
26 a	0.255	0.080	17.921	15.546	38.321	19.82
26 b	0.239	0.068	17.897	15.535	38.296	17.88
6 a	0.623	0.222	17.906	15.554	38.338	22.44
6 b	0.624	0.211	17.848	15.548	38.333	21.28

[a] Samples and sample numbers as in Fig. 3.
[b] Lead isotope analyses were performed at GeoForschungs-Zentrum Potsdam, Germany, using a Finnigan MAT262 multicollector mass spectrometer. The lead isotopic composition is corrected for mass discrimination with 0.1%/a.m.u. 2σ uncertainties are less than 0.1%. U and Pb concentrations were determined by ID-TIMS

(Table 6). All minerals show unusually high $^{87}Sr/^{86}Sr$ values when compared with most COMB granitoids (Stein 1985). Initial $^{87}Sr/^{86}Sr$ values of minerals from the Sweet Home Mine range between 0.73006 and 0.76038 (Table 6), whereas those of porphyry molybdenum granites/porphyries in the COMB range between 0.7049 and 0.7115 (White et al. 1981; Stein 1985). The Climax porphyry molybdenum deposit has $^{87}Sr/^{86}Sr$ values of 0.7099 to 0.7109 (Stein 1985). Wall rocks of the Tertiary granites and epithermal vein deposits typically have much more radiogenic $^{87}Sr/^{86}Sr$ values. For example, Proterozoic granites in Colorado show $^{87}Sr/^{86}Sr$ values (recalculated for the time of Sweet Home mineralization) ranging from 0.7115 (e.g., DePaolo 1981) to more radiogenic values, as high as 0.80 (White at al. 1981). It is noteworthy that all $^{87}Sr/^{86}Sr$ values in minerals from the Sweet Home mineralization are considerably more radiogenic than $^{87}Sr/^{86}Sr$ ratios of about 0.7105 reported from Climax plagioclase (Stein 1988). The $^{87}Sr/^{86}Sr$ values of Sweet Home fluorites are not uniform and scatter over a wide range (Fig. 11) suggesting that the fluids acquired a significant part of their Sr budget from wall rock alteration, i.e., by Sr-release from altered muscovite, biotite, and alkali-feldspar. The Sr isotopic composition of rhodochrosite and fluorite that precipitated during the main sulfide stage overlaps with the Sr isotopic composition of fluorite from the early stage. Despite the overlap of Sr isotopic compositions, there seems to be a general trend to more radiogenic Sr isotopic composition from older to younger minerals. The most radiogenic Sr isotopic composition is found for apatite which formed at the end of the main sulfide stage and is one of the youngest minerals at the Sweet Home Mine. The observed systematic increase of $^{87}Sr/^{86}Sr$ with time (and overall lower temperature, cf. Fig. 5), suggests that the influence of Sr from the wall rocks increases with time, i.e., the wall rock possibly became the dominant Sr source during the final stages of the hydrothermal system. The general trend to higher $^{87}Sr/^{86}Sr$ ratios with time, however, does not necessarily have to represent a simple mixing between different Sr sources (wall rock vs. magmatic fluids) but could reflect a change in the nature of wall rock minerals that were interacting with the fluids. If the proportion of high Rb/Sr phases had increased among the leached phases, the $^{87}Sr/^{86}Sr$ ratio in the mobilized fluid would also increase.

Discussion

Many characteristics of the mineralization at the Sweet Home Mine are comparable to those of the Oligocene and Miocene Climax-type deposits that developed within the COMB (e.g., Wallace et al. 1968; White et al. 1981; Bookstrom et al. 1987, 1988). Although high-grade quartz–molybdenite veins are lacking or have not been exposed by mining activity, the

Table 6 $^{87}Sr/^{86}Sr$ isotopic composition of apatite, fluorite, and rhodochrosite from the Sweet Home Mine, Colorado, U.S.A

Sample[a]	Rb[b] (ppm)	Sr[b] (ppm)	$\frac{^{87}Rb^{b}}{^{86}Sr}$	$\frac{^{87}Sr^{c}}{^{86}Sr}$	$\frac{^{87}Sr^{d}}{^{86}Sr}$ (T)
Apatite					
30				0.760117±7	
30				0.760181±7	
30				0.759576±7	
30				0.760260±7	
30				0.760375±6	
Hydrothermal rhodochrosite					
11	0.32	178	0.005	0.736973±7	0.73697
4	0.11	0.48	0.66	0.746873±25	0.74663
Hydrothermal Fluorite					
24	<0.3	61.7	0.014	0.751128±36	0.75112
25	1.07	141	0.022	0.748698±7	0.74869
24	<0.3	160	0.005	0.758628±19	0.75862
Greisen fluorite					
1	21.6	558	0.11	0.74700±7	0.7469
18	39.9	800	0.14	0.752299±17	0.75224
24	1.95	75.4	0.075	0.730059±17	0.73003
15	53.6	183	0.85	0.740209±11	0.73989

[a] Apatite samples represent fragments of a single late-stage apatite crystal used for U–Pb dating (Romer and Lüders, 2006). All other samples are aliquots of the powders used for chemical analysis

[b] Rb and Sr concentrations of the rhodochrosite and fluorite samples have been determined by ICP-MS. Sr and Rb concentrations of the apatite samples have not been determined

[c] Sr is normalized with $^{86}Sr/^{88}Sr=0.1194$

[d] The initial Sr isotopic composition has been calculated for T=26 Ma

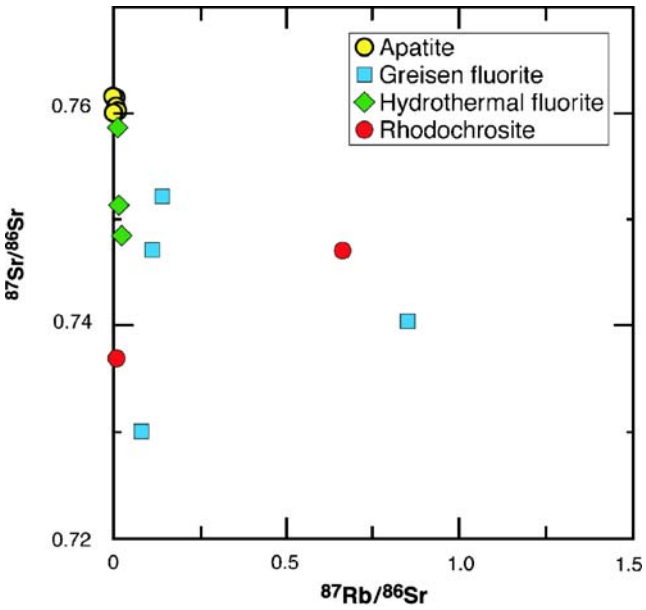

Fig. 11 $^{87}Rb/^{86}Sr$ vs. $^{87}Sr/^{86}Sr$ diagram for rhodochrosite, flourite, and apatite samples. Note that in situ Sr growth since the formation of veins some 27 m.y. ago can not account for the isotopic heterogenity between different minerals. Data from Table 6

mineralization at the Sweet Home Mine is mineralogically and paragenetically similar to the mineralization at the Climax deposit that is related to the intrusion of the Climax stock and late rhyolite porphyry dikes (Bookstrom 1989). For unaltered samples from the Climax Mo deposit, geochemical data, including Pb, O, S (Stein and Hannah 1985) and Sr isotopes and REE distribution (Stein 1988) suggest that the formation of quartz–molybdenite mineralization is related directly to magmatic fluids without a wall rock source component. Similarly, magmatic–hydrothermal fluids that were released from rhyolitic stocks are assumed to be the principle source for all metals and mineralization at the Henderson porphyry system, where high-temperature Mo mineralization was followed by moderate-temperature W and lower temperature Pb–Zn–(rhodochrosite–fluorite) mineralization (Seedorff and Einaudi 2004b).

Analogous to the large Mo porphyry deposits of the COMB, a magmatic origin for the early-stage quartz–molybdenite–pyrite–topaz–muscovite–fluorite mineralization at the Sweet Home Mine is supported by our geochemical data. The sulfur isotopic composition of pyrite ($\delta^{34}S \approx 1.7‰$) from the early stage of the Sweet Home mineralization is similar to values reported from the nearby Climax Mo deposit (Stein and Hannah 1985). The REY distribution patterns of early-stage fluorite are also in accordance with a model that invokes an origin of REE and Y from a felsic magmatic source (Bau and Dulski 1995). Fluid inclusions in quartz show an evolution from medium- (early milky quartz) to low-salinity (clear and euhedral quartz). The salinity of magmatic–hydrothermal fluids being released from crystallizing melts should decrease during fluid exsolution from the melt at any pressure above about 1.3 kbars (Cline and Bodnar 1994).

The question still remains why the fluids at the Sweet Home Mine show such a low metal content when compared with fluid inclusion data reported from other porphyry deposits (e.g., Bodnar 1995; Cline and Vanko 1995; Audétat at al. 2000; Landtwing et al. 2005; Klemm et al. 2008). However, halite-bearing fluid inclusions that are observed at Climax and are characteristic of magmatic fluids in porphyry-type deposits (Roedder and Bodnar 1997) are absent at Sweet Home. We suggest that the high-salinity fluids that would have generated halite-bearing inclusions were present at depth beneath the Sweet Home deposit but were either stored at depth or were diluted by externally derived fluids as they migrated upwards to the level of the Sweet Home deposit. Such a model requires phase separation of the exsolving magmatic fluids at some depth beneath the present-day mining level of the Sweet Home Mine. The low metal content (except Cu) of the fluid inclusions is also consistent with a model that involves boiling of magmatic fluids at some depth below the Sweet Home Mine. As has been observed in porphyry copper deposits, the vapor produced by boiling would contain significant amounts of Cu but would be depleted in most other metals (e.g., Bodnar 1992; Heinrich et al. 1999; Heinrich 2007). Fluids trapped in early quartz may thus represent condensates of vapors and/or mixtures of externally derived fluids with condensed magmatic vapor.

Mineralization at the Sweet Home Mine includes hübnerite-bearing veins and pockets, similar to the Henderson and Climax deposits. At the Climax deposit, tungsten-bearing mineralization is younger than Mo-bearing veinlets (Wallace and Bookstrom 1993). The paragenetic position of hübnerite mineralization at the Sweet Home Mine is not clear (Misantoni et al. 1998; Bartos et al. 2007). It may either be associated with the early mineralization stage or is transitional between the early stage and main sulfide stage. However, three hübnerite samples define a $^{206}Pb/^{238}U$ age of 25.7±0.3 Ma (2σ; Romer and Lüders 2006), which corresponds with the $^{40}Ar/^{39}Ar$ ages of sericite (Barbá et al. 2005) indicating that there was not a long gap between the formation of early quartz–molybdenite–pyrite–topaz–muscovite–fluorite mineralization and the deposition of hübnerite. The homogenization temperatures of hübnerite-hosted fluid inclusions are similar to those of early-stage quartz (Fig. 5). Since hübnerite always grows on quartz a simple cooling model for the precipitation of quartz and hübnerite from the same fluids is unlikely, although this process has been suggested for the hübnerite mineralization at Henderson (Seedorf and Einaudi 2004b). Furthermore, aqueous, low-carbonic type 2 inclusions that are characteristic of quartz–molybdenite–pyrite–topaz–muscovite–fluorite

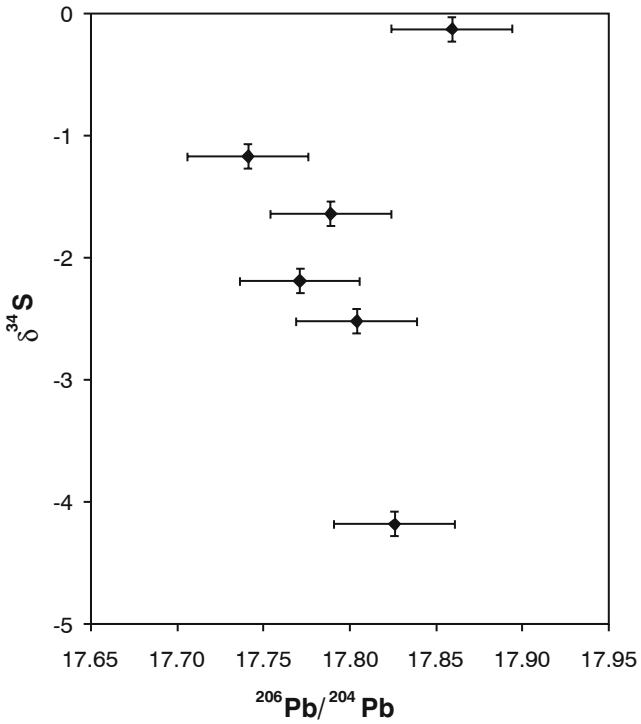

Fig. 12 $^{206}Pb/^{204}Pb$ vs. δ^{34} S diagram for galena samples from the main sulfide stage

mineralization have not been detected in hübnerite at Sweet Home. Instead, some hübnerite samples contain nitrogen-bearing inclusions. Nitrogen may have been derived from decrepitated inclusions in the crystalline basement rocks, or released during metamorphic dehydration processes (Jia and Kerrich 1999; Mingram and Bräuer 2001), or exchanged with feldspars and/or micas during fluid–rock interaction at elevated temperatures; i.e., replacement of NH_4^+ by K^+ (e.g., Pötter et al. 2004).

The main sulfide stage at the Sweet Home Mine is characterized by the deposition of various Pb–Zn–Cu–Ag–As–Sb sulfides with fluorite and rhodochrosite as common gangue minerals. Calcite, barite, and apatite were the last minerals to form. Generally, homogenization temperatures, salinity, and CO_2 content of fluid inclusions decrease with progressive mineral deposition probably indicating the exhaustion of the magmatic fluid input (Table 1 and Fig. 5). The Pb isotopic compositions of galena, rhodochrosite, and apatite suggest different sources for lead compared to that of the Oligocene granitoids. Climax-type granites in the COMB are assumed to have Pb from lower crustal sources (Stein and Hannah 1985; Stein 1988). The $^{207}Pb/^{204}Pb$ ratios (Fig. 10) of galena from the main sulfide stage, however, are much higher than those reported for

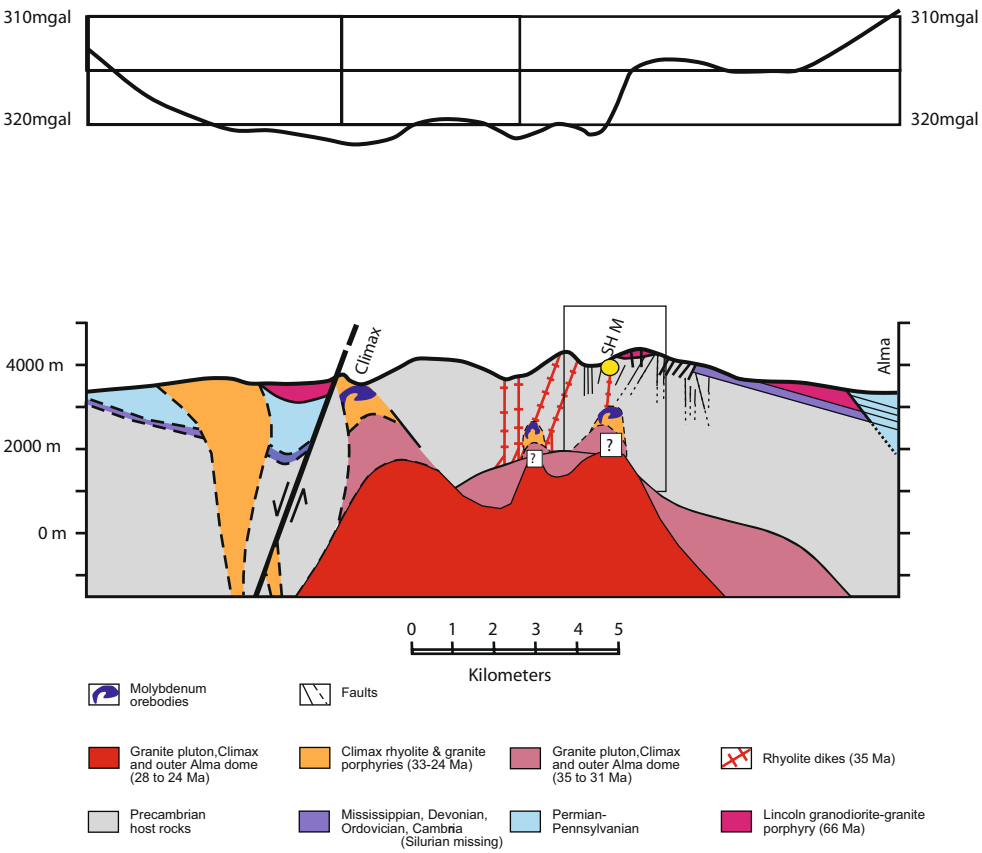

Fig. 13 Geologic section and Bouger gravity anomaly profile across the Climax and Alma districts (after Bookstrom et al. 1988, and Bookstrom 1989). The Sweet Home mineralization has previously been interpreted to be related to magmatic activity that formed the inner Alma dome at about 24 to 28 Ma (Bookstrom et al. 1988; Bookstrom 1989). We propose that a hidden Mo porphyry deposit in a satellite intrusion of the Alma Batholith may be located below the Sweet Home system, similar to the currently exposed Climax Mo deposit

galena from the COMB and suggest a different old crustal source for lead. There is also a correlation between increasing $^{206}Pb/^{204}Pb$ ratios of galena and decreasing $\delta^{34}S$ isotopic composition (Fig. 12) which suggests (with only one exception) progressive water/rock interaction between meteoric fluids and crustal rocks and the release of lead and sulfur. In contrast, the $^{207}Pb/^{204}Pb$ ratios of rhodochrosite and apatite from the main sulfide stage fall in the range of lead isotope data for the COMB (Fig. 10). This may suggest mixing of magmatic fluids with externally derived fluids that have leached old crustal lead from the Precambrian basement. Mixing of magmatic fluids with meteoric water is also evidenced by the C and O isotopic relationship in rhodochrosite (Fig. 9). Furthermore, the high Y/Ho ratio but low REE content of fluorite from the main sulfide stage also support a model that involves large-scale fluid migration and alteration of the crystalline basement rather than an exclusive fluid origin from felsic magmatic rocks. Finally, the highly variable $^{87}Sr/^{86}Sr$ ratios of fluorite, rhodochrosite, and apatite indicate that at least part of the Sr originated from a much more radiogenic source than observed in Climax-type granites (Stein 1988). All these features suggest that the hydrothermal fluids that deposited ore and gangue minerals during the main sulfide stage at the Sweet Home Mine, which is regarded to be an analogue of low-temperature base metal mineralization peripheral to Mo ore bodies at the Climax and Henderson deposits, are not exclusively of magmatic origin (Stein 1988; Bookstrom 1989; Seedorff and Einaudi 2004b). The fluids also are unlikely to represent mixtures of primarily magmatic fluids with minor amounts of meteoric water (Bartos et al. 2007). Instead, it is more likely that deeper seated magmatic intrusion(s) triggered large-scale convection of externally derived fluids that interacted extensively with the crystalline basement and/or country rocks and mixed to varying proportions with ascending magmatic fluids.

Summary and geologic model

The hydrothermal mineralization at the Sweet Home Mine has both magmatic and externally derived fluid sources. Geophysical data are consistent with the presence of a small apophysis off of the Alma Batholith in the subsurface in the vicinity of the Sweet Home Mine (Fig. 12). A similar and much larger satellite body from the same Alma Batholith is associated with the Climax molybdenum deposit (e.g., Bookstrom 1989). The Climax deposit is located at about 2 km higher elevation compared to the top of the inferred apophysis beneath the Sweet Home deposit. Thus, we would expect that any large-scale molybdenum mineralization associated with the apophysis at Sweet Home would be located some 2 km beneath the present surface (Fig. 13).

The deposition of early-stage quartz–molybdenite–pyrite–topaz–muscovite–fluorite mineralization, which is an analogue to Climax-type Mo mineralization, was dominated by moderately saline, magmatic fluids with CO_2 at around 400°C, The pressure regime fluctuated from high to lower pressure during the formation of early milky quartz through euhedral quartz, probably as a result of sealing and re-opening of fractures. REY distribution and Sr isotopic composition in fluorite from the early stage support an interpretation of a fluid origin from a felsic magma source. The magmatic fluid probably exsolved from a differentiated melt, highly enriched in volatiles, and incompatible elements such as Rb and Cs.

The formation of abundant sulfide mineralization with fluorite and rhodochrosite as gangue minerals is similar to peripheral epithermal mineralization at the Climax and Henderson Mo deposits. The Sweet Home base metal mineralization was produced by mixing of externally derived fluids with magmatic fluids as evidenced by mostly negative $\delta^{34}S$ values of sulfides, highly variable $\delta^{18}O$ values of rhodochrosite, and low REE content in fluorite. The Pb isotopic composition of galena as well as the highly variable $^{87}Sr/^{86}Sr$ ratios of fluorite, rhodochrosite, and apatite indicate that most of the Pb and Sr originated from a significantly more radiogenic source than observed in Climax-type granites. Sulfide mineralization was deposited from low-salinity $\pm CO_2$-bearing fluids below 400°C, probably under hydrostatic pressure conditions.

If the conclusion holds that the Sweet Home Mine mineralization is the uppermost expression of a hidden molybdenum porphyry system, then the deep area beneath Sweet Home would represent an attractive exploration target.

Acknowledgments We are most grateful to Bryan Lees (Collector's Edge, Golden, CO) for providing numerous fascinating mineral specimens and detailed information. Special thanks go to T. James Reynolds (Denver) and Bernd Lehmann (Clausthal) for constructive comments. We are indebted to P. Dulski (GFZ Potsdam) for REY analysis and H. Strauß (University Münster) for sulfur isotope analysis. We thank G. Berger (GFZ) for preparing numerous doubly polished thick sections.

References

Audétat A, Pettke T (2003) The magmatic–hydrothermal evolution of two barren granites: a melt and fluid inclusions study of the Rito del Medio and Cañada Pinabete plutons in northern New Mexico (USA).. Geochim Cosmochim Acta 67::7–121

Audétat A, Günther D, Heinrich CA (2000) Causes for large-scale metal zonation around mineralized plutons: fluid inclusion LA-ICPMS evidence from the mole granite, Australia. Econ Geol 95:1563–1581

Bakker RJ, Dubessy J, Cathelineau M (1996) Improvements in clathrate modelling: I. The H_2O–CO_2 system with various salts. Geochim Cosmochim Acta 60:1657–1681

Barbá KE, Nelson EP, Misantoni D, Hitzman MW, Layer PW (2005) Structural controls on mineralized veins in the Sweet Home Mine, Alma district, Colorado. In: Rhoden HN, Steininger RC and Vikre PG (eds) Geol Soc Nevada Symp 2005: 698–708

Barton PB, Chou I-M (1993) Calculation of the vapor-saturated liquidus for the NaCl–CO_2–H_2O system. Geochim Cosmochim Acta 57:2715–2723

Bartos PJ, Nelson EP, Misantoni D (2007) The Sweet Home rhodochrosite specimen mine, Alma District, Central Colorado: the porphyry molybdenum-fluorine connection. Miner Deposita 42:235–250

Bau M (1996) Controls on the fractionation of isovalent trace elements in magmatic and aqueous systems: evidence from Y/Ho, Zr/Hf, and lanthanide tetrad effects. Contrib Mineral Petrol 123:323–333

Bau M, Dulski P (1995) Comparative study of yttrium and rare-earth element behaviour in fluorine-rich hydrothermal fluids. Contrib Mineral Petrol 119:213–223

Bau M, Möller P (1992) Rare earth element fractionation in metamorphogenic hydrothermal calcite, magnesite and siderite. Mineral Petrol 45:231–246

Bethke PM, Rye RO (1979) Environment of ore deposition in the Creede mining district, San Juan Mountains, Colorado: part IV. source of fluids from oxygen, hydrogen and carbon isotopes. Econ Geol 74:1832–1851

Bodnar RJ (1992) Can we recognize magmatic fluid inclusions in fossil hydrothermal systems based on room temperature phase relations and microthermometric behavior? Geol Surv Japan, Rep 279:26–30

Bodnar RJ (1993) Revised equation and table for determining the freezing point depression of H_2O–NaCl solutions. Geochim Cosmochim Acta 57:683–684

Bodnar RJ (1995) Fluid inclusion evidence for a magmatic source for metals in porphyry copper deposits. In: Magmas. fluids and ore deposits (Thompson JFH, ed) Canada Short Course Vol 23:139–152.

Bodnar RJ, Reynolds TJ, Kuehn CA (1985) Fluid inclusion systematics in epithermal systems. In: Berger BR and Bethke PM (eds) Geology and geochemistry of epithermal systems. Rev Econ Geol 2:73–97

Bookstrom AA (1989) The Climax-Alma granite batholith of Oligocene age and the porphyry molybdenum deposits of Climax, Colorado, U.S.A. Eng Geol 27:543–568

Bookstrom AA, Naeser CW, Shannon JR (1987) Isotopic age determinations, unaltered and hydrothermally altered igneous rocks, north-central Colorado Mineral Belt. Isochron W 49:13–20

Bookstrom AA, Carten RB, Shannon JR, Smith RP (1988) Origin of bimodal leucogranite-lamprophyre suites, Climax and Red Mountain porphyry molybdenum systems, Colorado: petrographic and strontium isotope evidence. CO School of Mines Quarterly 83:1–24

Böttcher ME (1993) Die experimentelle Untersuchung Lagerstätten-relevanter Metall-Anreicherungen aus wäßrigen Lösungen unter besonderer Berücksichtigung von Rhodochrosit ($MnCO_3$). Diss Univ Göttingen. 237 p.

Casadevall T, Ohmoto H (1977) Sunnyside mine, Eureka mining district, San Juan County, Colorado: Geochemistry of gold and base metal ore deposition in a volcanic environment. Econ Geol 72:1285–1320

Cline JS, Bodnar RJ (1994) Direct evolution of brine from a crystallizing silicic melt at the Questa, New Mexico, molybdenum deposit. Econ Geol 89:1780–1802

Cline JS, Vanko DA (1995) Magmatically generated saline brines related to molybdenum at Questa, New Mexico, USA. In: Magmas. fluids and ore deposits (Thompson JFH, ed) Min Ass Canada Short Course Vol 23:153–174

Deines P (2004) Carbon isotope effects in carbonate systems. Geochim Cosmochim Acta 68:2659–2679

DePaolo DJ (1981) Neodymium isotopes in the Colorado front range and crustal mantle evolution in the Proterozoic. Nature 291:193–196

Diamond LW (1994) Introduction to phase reactions of CO_2–H_2O fluid inclusions. In: De Vivo B, Frezotti ML (eds) Fluid inclusions in minerals: methods and application. Virginia Tech, Blacksburg, pp 131–158

Doe BR, Zartman RE (1979) Plumbotectonics, the Phanerozoic. In: Barnes HL (ed) Geochemistry of hydrothermal ore deposits (2nd ed). 22–70

Dulski P (2001) Reference materials for geochemical studies: new analytical data by ICP-MS and critical discussion of reference values. Geost Newsl, J Geostand Geoanal 25:87–125

Evensen NH, Hamilton PJ, O'Nions RK (1978) Rare-earth abundances in chondritic meteorites. Geochim Cosmochim Acta 42:1199–1212

Günther D, Audeta A, Frischknecht R, Heinrich CA (1998) Quantitative analysis of major, minor and trace elements in fluid inclusions using laser ablation inductively coupled plasma mass spectrometry. J Anal Atom Spec 13(4):263–270

Goldstein RH, Reynolds TJ (1994) Systematics of fluid inclusions in diagenetic minerals. SEPM Short C 31:1–199

Hall WE, Friedmann I, Nash JT (1974) Fluid inclusion and light stable isotope study of the Climax molybdenum deposit, Colorado. Econ Geol 69:884–901

Heinrich CA (2007) Fluid–fluid interactions in magmatic–hydrothermal ore formation. In Liebscher A, Heinrich CA (eds) Fluid–fluid interactions. Mineral Soc Am, Rev Mineral 65:363–387

Heinrich CA, Günther D, Audétat A, Ulrich T, Frischknecht R (1999) Metal fractionation between magmatic brine and vapor, determined by microanalysis of fluid inclusions. Geol 32:761–764

Heinrich CA, Pettke T, Halter WE, Aigner-Torres M, Audétat A, Günther D, Hattendorf B, Bleiner D, Guillong M, Horn I (2003) Quantitative multi-element analysis of minerals, fluid and melt inclusions by laser-ablation inductively-coupled-plasma mass-spectrometry. Geochim Cosmochim Acta 67:3473–3496

Jia Y, Kerrich R (1999) Nitrogen isotope systematics of mesothermal lode gold deposits; metamorphic, granitic, meteoric water, or mantle origin? Geol 27:1051–1054

Klemm LK (2006) Cu–Mo–Au ratios in porphyry-type ore deposits: constraints from fluid inclusion microanalysis. PhD thesis ETH Zürich No. 16396. http://e-collection.ethbib.ethz.ch/show?type=diss&nr=16395

Klemm LK, Pettke T, Heinrich CA (2008) Fluid and source magma evolution of the Questa porphyry Mo deposit, New Mexico, USA. Miner Dep 43:533–552

Landtwing MR, Pettke T, Halter WE, Heinrich CA, Redmond PB, Einaudi MT, Kunze K (2005) Copper deposition during quartz dissolution by cooling magmatic-hydrothermal fluids: The Bingham porphyry. Earth Planet Sci Lett 235:229–243

Kelley KD, Ludington S (2002) Cripple creek and other alkaline-related gold deposits in the southern Rocky Mountains, USA: influence of regional tectonics. Min Dep 37:38–60

Lüders V (1996) Contribution of infrared microscopy to fluid inclusion studies in some opaque minerals (wolframite, stibnite, bournonite): metallogenetic implications. Econ Geol 91:1462–1468

Lüders V, Möller P, Dulski D (1993) REE fractionation in carbonates and fluorite. Monogr Ser Mineral Dep 30:133–150

Mingram B, Bräuer K (2001) Ammonium concentration and nitrogen isotope composition in metasedimentary rocks from different tectonometamorphic units of the European Variscan Belt. Geochim Cosmochim Acta 65:273–287

Misantoni D, Silbermann ML, Lees BK (1998) Geology of the Sweet Home Mine and Alma district. Mineral Rec 29:101–114

Möller P, Bau M, Dulski P, Lüders V (1998) REE and yttrium fractionation in fluorite and their bearing on fluorite formation. Proc 9th Quadr IAGOD Symp, pp 575–592

Moore T, Lees BK, Wenrich KJ, Voynick S, Murphy JA, Hurlbut JF, Reynolds TJ, Aumente-Modreski R, Misantoni D, Silberman ML (1998) The Sweet Home Mine, park county, Colorado. Mineral Rec 29:192

Ohmoto H, Rye RO (1979) Isotopes of sulfur and carbon. In: Barnes HL (ed) Geochemistry of hydrothermal ore deposits, . nd edn. 2nd edn. Wiley, New York, pp 509–567

Pettke T, Halter WE, Webster JD, Aigner-Torres M, Heinrich CA (2004) Accurate quantification of melt inclusion chemistry by LA-ICPMS: a comparison with EMP and SIMS and advantages and possible limitations of these methods. Lithos 78:333–361

Pötter B, Gottschalk M, Heinrich W (2004) Experimental determination of the ammonium partitioning among muscovite, K-feldspar, and aqueous chloride solutions. Lithos 74:67–90

Reynolds TJ (1998) Ancient fluids at the Sweet Home Mine. Mineral Rec 29:127–132

Roedder E (1984) Fluid inclusions. Mineral Soc Am Rev Mineral 12:1–644

Roedder E, Bodnar RJ (1980) Geologic pressure determinations from fluid inclusion studies. Ann Rev Earth Planet Sci 8:263–301

Roedder E, Bodnar RJ (1997) Fluid inclusion studies of hydrothermal ore deposits. In: Barnes HL (ed) Geochemistry of hydrothermal ore deposits. 3rd edn. Wiley, New York, pp 657–698

Romer RL, Lüders V (2006) Direct dating of hydrothermal W mineralization: U–Pb age for hübnerite (MnWO4), Sweet Home Mine, Colorado. Geochim Cosmochim Acta 70:4725–4733

Romer RL, Heinrich W, Schröder-Smeibidl B, Meixner A, Fischer C-O, Schulz C (2005) Elemental dispersion and stable isotope fractionation during reactive fluid-flow and fluid immiscibility in the Bufa del Diente aureole, NE-Mexico: Evidence from radiographies and Li, B, Sr, Nd, and Pb isotope systematics. Contrib Mineral Petrol 149:400–429

Seedorff E, Einaudi MT (2004a) Henderson porphyry molybdenum system, Colorado: I. Sequence and abundance of hydrothermal mineral assemblages, flow paths of evolving fluids, and evolutionary style. Econ Geol 99:3–37

Seedorff E, Einaudi MT (2004b) Henderson porphyry molybdenum system, Colorado: II. Decoupling of introduction and deposition of metals during geochemical evolution of hydrothermal fluids. Econ Geol 99:39–72

Stein HJ (1985) A lead strontium, sulphur isotopic study of Laramide-Tertiary intrusions and mineralization in the Colorado mineral belt with emphasis on climax-type porphyry molybdenum systems plus a summary of other newly acquired isotopic and rare earth element data. PhD Diss, Univ North Carolina, Chapel Hill, pp. 493

Stein HJ (1988) Genetic traits of Climax-type granites and molybdenum mineralization, Colorado Mineral Belt. In: Taylor RP and Strong DF (eds) Recent advances in the geology of granite-related mineral deposits. Can Inst Min Metal Spec Vol 39:394–401

Stein HJ, Crock JG (1990) Late Cretaceous–Tertiary magmatism in the Colorado Mineral Belt: rare earth element and samarium–neodymium isotopic studies. Geol Soc Am Mem 174:195–223

Stein HJ, Hannah JL (1985) Movement and origin of ore fluids in Climax-type systems. Geol 13:469–474

Sterner SM, Bodnar RJ (1984) Synthetic fluid inclusions in natural quartz. I. Compositional types synthesized and applications to experimental geochemistry. Geochim Cosmochim Acta 48:2659–2668

Taylor SR, McLennan SM (1985) The continental crust: its composition and evolution. Blackwell, Oxford

Thomas R, Förster HJ, Rickers K, Webster JD (2005) Formation of extremely F-rich hydrous melt fractions and hydrothermal fluid during differentation of highly evolved tin-granite magmas: a melt fluid inclusion study. Contr Mineral Petrol 148:582–601

Wallace SR (1995) The climax-type molybdenum deposits: what they are, where they are, and why they are. Econ Geol 90:1359–1380

Wallace SR, Bookstrom AA (1993) The Climax molybdenum system. CO School of Mines Quart Rev 93:35–41

Wallace SR, MacKenzie WB, Blair RG, Muncaster NK (1978) Geology of the Urad and Henderson molybdenite deposits, Clear Creek County, Colorado, with a section on a comparison of these deposits with those at Climax, Colorado. Econ Geol 73:325–368

Wallace SR, Muncaster NK, Jonson DC, MacKenzie WB, Bookstrom AA, Surface VE (1968) Multiple intrusion and mineralization at Climax, Colorado. In: Ridge JD (ed) Ore deposits of the United States 1933–1967. New York, Am Inst Min, Metall, Petrol Engin pp. 605–640

Westra G, Keith SB (1981) Classification and genesis of stockwork molybdenum deposits. Econ Geol 76:844–873

White WH, Bookstrom AA, Kamilli RJ, Ganster WM, Smith RP, Ranta DE, Steininger RC (1981) Character and origin of Climax-type molybdenum deposits. Econ Geol 75th Anniv Vol:270–316

Zartman RE, Doe BR (1981) Plumbotectonics—the model. Tectonophys 75:135–162